A Library of Integrated Spectra of Galactic Globular Clusters

Ricardo P. Schiavon

Astronomy Department, University of Virginia, P O Box 3818, Charlottesville, VA 22903, USA

ripisc@virginia.edu

James A. Rose

Department of Physics & Astronomy, University of North Carolina, Chapel Hill, NC 27599, USA

jim@physics.unc.edu

Stéphane Courteau

Department of Physics, Queen's University, Kingston, ON K7L 3N6, Canada

courteau@astro.queensu.ca

and

Lauren A. MacArthur

Department of Physics & Astronomy, University of British Columbia, 6224 Agricultural Road, Vancouver, BC Canada, V6T 1Z1

lauren@physics.ubc.ca

ABSTRACT

We present a new library of integrated spectra of 40 Galactic globular clusters, obtained with the Blanco 4-m telescope and the R-C spectrograph at the *Cerro Tololo Interamerican Observatory*. The spectra cover the range $\sim$ 3350 – 6430 Å with $\sim$ 3.1 Å (FWHM) resolution. The spectroscopic observations and data reduction were designed to integrate the full projected area within the cluster core radii in order to properly sample the light from stars in all relevant evolutionary stages. The S/N values of the flux-calibrated spectra range from 50 to 240/Å at 4000 Å and from 125 to 500/Å at 5000 Å. The selected targets span a wide range of cluster parameters, including metallicity, horizontal-branch morphology, Galactic coordinates, Galactocentric distance, and concentration. The

total sample is thus fairly representative of the entire Galactic globular cluster population and should be valuable for comparison with similar integrated spectra of unresolved stellar populations in remote systems. For most of the library clusters, our spectra can be coupled with deep color-magnitude diagrams and reliable metal abundances from the literature to enable the calibration of stellar population synthesis models. In this paper we present a detailed account of the observations and data reduction. The spectral library is publicly available in electronic format from the National Optical Astronomical Observatory website.

Subject headings: globular clusters: general; galaxies: evolution

1. Introduction

The determination of the stellar content of unresolved systems from observations of their integrated light is a fundamental challenge to extragalactic astronomers. The problem has been traditionally approached by comparing the integrated properties (spectral energy distributions, line strengths, colors) of remote systems with those of better-understood local templates (e.g. Faber 1973, Burstein et al. 1984, Rose 1985). More recently, stellar population synthesis (SPS) models combined with our knowledge of the stellar evolution of stars and of the behaviour of their emitted light as a function of fundamental stellar parameters have been constructed to predict integrated properties of single and composite stellar populations in integrated light (e.g. Le Borgne et al. 2004, Bruzual & Charlot 2003, Thomas, Maraston & Bender 2003, Vazdekis 1999, Worthey 1994).

In this context, the Galactic globular cluster (GC) system plays a crucial role. It consists of a set of increasingly well studied stellar populations which are close enough that their constituent stars can be resolved and studied individually and meaningful color-magnitude diagrams can be constructed, and yet their compact structures enable observations of their integrated light relatively easily. Integrated observations of GCs can be used to construct calibrations of integrated observables as a function of the parameters that characterize stellar populations (mainly age, metallicity, and abundance pattern). Such calibrations provide useful, fairly model-independent tools for the conversion of integrated observables of distant systems into fundamental stellar population parameters. Moreover, comparisons of SPS models with integrated observations of Galactic GCs has become commonplace (e.g. Proctor, Forbes & Beasley 2004, Schiavon et al. 2004a,b, Maraston et al. 2003, Puzia et al. 2002, Schiavon et al. 2002a,b, Beasley, Hoyle & Sharples 2002, Vazdekis et al. 2001, Gibson et al. 1999, Schiavon & Barbuy 1999, Bruzual et al. 1997, Rose 1994, and references therein). Such fundamental comparisons aim primarily at verifying the validity of the models, whose

predictions must match the integrated properties of GCs for the known set of input stellar population parameters.

Reliable databases of integrated properties of Galactic GCs are therefore precious resources and numerous efforts have been invested towards their collection in the past. Notable among these are the works of Puzia et al. (2002), Cohen, Blakeslee & Ryzhov (1998), Covino, Galletti & Pasinetti (1995), Bica & Alloin (1986), Burstein et al. (1984), and Zinn & West (1984), where integrated spectra of moderate to large-sized samples of Galactic GCs were collected. In spite of these and other previous works, there remains considerable room for improvement to the available spectroscopic databases which are deficient in one or more of such crucial features as size, a representative range of metallicities and horizontal branch (HB) morphologies, signal-to-noise ratio (S/N), resolution, and homogeneity. These features are all essential both for a robust calibration of stellar population synthesis models and for the direct comparison with observations of distant systems. This work aims at providing this much needed improvement.

We present new, high-S/N, moderately high-resolution, integrated spectra of 40 Galactic globular clusters obtained with the same instrumental setup and over a single observing run. This is the largest collection of optical integrated spectra of Galactic GCs to date with such high S/N and resolution, and should serve as a prime database for comparison with observations of remote stellar systems and the calibration of SPS models. This paper focuses on the detailed description of our observations and data reduction procedures, and the presentation of the final data products. A first exploration of this spectral library, focussed on the effects of HB morphology on different Balmer lines, was presented in Schiavon et al. (2004b).

The paper is organized as follows: we describe the sample selection and observations, in Sections 2 and 3, respectively, and the reductions are discussed in Section 4. The final spectra are presented in Section 5 and Section 6 contains notes on individual clusters. Our results are summarized in Section 7.

2. Sample Selection

Our choice of GC targets was chiefly aimed at producing a spectral library that is representative of the Galactic GC system. Therefore, GCs spanning a wide range of metallicities, HB morphologies, and Galactocentric distances were chosen. Another important consideration is that the spectral library will become more useful if GC characteristic parameters such as age, metallicity, and HB morphology are known accurately. Therefore, we gave priority

to GCs for which [Fe/H] values, based on abundance analyses of high resolution spectra of member stars (e.g. Carretta & Gratton 1997, Kraft & Ivans 2003), are available. For the same reason, we also preferred GCs for which high-quality color-magnitude diagrams, preferrably reaching below the turn-off, are available from the literature (e.g. Piotto et al. 2002). The combination of such data with our spectral library optimizes the construction of reliable calibrations of integrated GC properties with fundamental determinations of basic parameters like age, metallicity and HB morphology. The distribution of our GC sample in Galactic coordinates is shown in Figure 1.

The main characteristics of our globular cluster sample are summarized in Table 1. We list in columns (1) and (2) the cluster IDs, in columns (3) and (4) the positions in galactic coordinates, and in column (5) Galactocentric distances in kpc. In column (6) we list core radii, r_c, in arcminutes, in column (7) the central concentration parameter $c = \log(r_t/r_c)$, where r_t is the tidal radius, and in column (8) reddening values, $E(B-V)$, are listed. We list in column (9) [Fe/H] values from high-resolution abundance analyses, when available, and those determined by Schiavon et al. (2005, in preparation) otherwise. In column (10) the Lee, Demarque & Zinn (1994) parameter describing the morphology of the HB is listed. Finally, in column (11) we provide a non-exhaustive list of recent references where deep color-magnitude diagrams for the sample clusters can be found. The data in columns (3), (4), (5), and (8) were taken primarily from Piotto et al. (2002), or otherwise from the compilations by Djorgovski & Meylan (1993), Djorgovski (1993), and Peterson (1993). The [Fe/H] values from Schiavon et al. (2005, in preparation) are derived from a new metallicity scale for Galactic GCs, based on measurements of iron absorption lines and state-of-the-art high-resolution abundance analyses of cluster members. The HB morphologies listed in column (10) were taken from Borkova & Marsakov (2000). For GCs whose HB morphologies are not given by Borkova & Marsakov, we provide qualitative estimates from inspection of the color-magnitude diagrams of Piotto et al. (2002). Core radii and concentration parameters were taken from Harris (1996) (`http://physwww.mcmaster.ca/~harris/mwgc.dat`).

3. Observational Data

3.1. Instrumental Setup

All observations were obtained with the Ritchey-Chretien spectrograph mounted on the 4-m Blanco telescope at the *Cerro Tololo Inter-American Observatory* (CTIO) on the nights of 24-27 April 2003. A Loral 3K x 1K CCD detector was used with an Arcon controller. The grating KPGL#1, with 632 grooves/mm, was used in first order with the blue collimator, yielding a dispersion of 1.0 Å/pix over the wavelength range 3360–6430 Å. A spectral

resolution of 3.1 Å FWHM was achieved in the central ∼1000 Å of the dispersion curve, deteriorating to ∼3.6 Å FWHM at the blue and red ends of the spectrum. A cubic polynomial fit to the FWHM of arc lines as a function of wavelength produced the following curve:

$$FWHM = 15.290 - 6.079 \times 10^{-3}\lambda + 9.472 \times 10^{-7}\lambda^2 - 4.395 \times 10^{-11}\lambda^3, \quad (1)$$

where λ is the wavelength. Both FWHM and λ are given in Å.

The spectra were binned by a factor of two along the slit, yielding a spatial scale of 1″ /pixel. The gain of the CCD was set to 1.0 e^-/ADU, and the read noise was determined to be 7.3 e^-. For all observations, except those of flux standards, the slit width was set at 225 μm or 1.″5. However, as we discuss further in §3.5, there were problems with the slit width in the second half of the last night of observations, due to a failure in the slit motor and its subsequent reinitialization. The change in slit width also produced a change in spectral resolution for those observations. For the first two nights, the ∼ 5.′5-long slit was oriented in the North-South direction, and was along the East-West direction for the final two nights.

3.2. Calibration Exposures

At the beginning of each night a sequence of 25 bias frames and 25 dome flat field frames were acquired. The bias level fluctuated throughout the observing run, but could always be subtracted adequately (see §3.5). Twilight exposures were recorded on the first two nights to provide illumination correction along the slit. The combination of a set of 5 arc lamp exposures taken at the beginning of each night provided a high-S/N master arc. Finally, on the last night, we observed the G star HD76151 at several positions along the slit to aid in mapping optical distortions in the spectrograph. Specifically, we observed HD76151 at the center of the slit, and repeated the observation with the slit offset by 1′, 2′, and 2.′5 East and West of the central position.

3.3. Globular Cluster Observations

Due to the spatially extended nature of globular clusters, and our desire to obtain their representative integrated spectra, each globular cluster observation was obtained by drifting the spectrograph slit across the core diameter of the cluster. The cluster core radii are listed in Table 1. The telescope was positioned so as to offset the slit from the cluster center by one core radius. A suitable trail rate would then allow the slit to drift across the cluster core

diameter during the typically 15 minute-long exposure.

In addition to the trail across the cluster core, a suitable background determination is required. We considered the extraction of a background spectrum from the ends of the $\sim 5\farcm5$ slit. However there are several disadvantages to this procedure. For many of the clusters, there would still be significant contamination from the cluster itself even at a radial distance of $\sim$2–3′. Use of the extreme ends of the slit for sky subtraction also requires a very secure mapping of the slit illumination and of the geometric distortions in the spectrograph. As well, there is the danger of deteriorating focus at large distances from the slit center. All of these problems are circumvented by taking a separate sky exposure from the cluster exposure, and then directly subtracting the sky frame from the cluster frame[1]. This approach also allows one to carefully select patches of background that appear to be well matched to that of the cluster, which is particularly important in regions towards the Galactic bulge, where the background variations are large due to non-uniform extinction and/or diffuse HII emission. We selected background areas in the vicinity of each cluster from film copies of the *European Southern Observatory/SRC* plates and/or print copies of the *Palomar Observatory Sky Survey*. In crowded regions towards the Galactic bulge, areas of typically $5' \times 5'$ or $10' \times 10'$ were selected for background scans. The criteria used in defining the scan region included visually similar level of faint background stars as for the cluster, avoidance of discrete bright stars, and, if applicable, similar level of HII emission as the cluster (as best seen on the red sky survey print/film).

The typical observation sequence included an arc spectrum, a 15 minute trailed cluster observation, and a 15 minute trailed background observation. For clusters with a low star background, the slit was fixed at a particular sky position, i.e., no trail was made for the background spectrum. In the case of one cluster, NGC 6352, for which the background spectrum was "contaminated" by the presence of several very bright B and A stars that were covered in the trailed background spectrum, we found it safer to use the ends of the slit from the cluster observation to extract the background spectrum. A journal of observations, providing complete information regarding the globular cluster and background spectra, is given in Table 2. We give in columns (1), (2), and (3) the cluster IDs, the UT date of observation, and the exposure time (in minutes), respectively. The orientation of the spectrograph slit is listed in column (4). In column (5) we specify the angular distance, in arcseconds, over which the spectrograph slit was trailed. A trail of 50″ indicates that we trailed by ±25″ on either side of the cluster center. We list in columns (6) and (7) the exposure time and angular offset

[1]This procedure is of course only recommended when the sky background does not fluctuate significantly in timescales comparable to the exposure times, a condition that is met in the optical, but not, for instance, in the near-infrared.

(from the cluster center), in arcminutes, for the sky background exposure. In column (8) we give the angular distance, in arcminutes, over which we trailed the spectrograph slit for the sky background exposure. A trail of $10'$ indicates that we moved the telescope by $\pm 5'$on either side of the sky offset position given in column (7). Finally, in column (9) we give the region extracted along the slit for the given cluster. Normally this was a symmetrical extraction of $\pm r_c$ on either side of the cluster center, but in some instances it was necessary to consider an asymmetrical extraction.

3.4. Standard Star Observations

In addition to the globular cluster observations, typically 2 or 3 spectrophotometric flux standards were observed per night. For these observations the slit was widened to $10''$to avoid wavelength-dependent light losses through differential atmospheric refraction. For the cluster observations the slit was trailed across the cluster so that atmospheric dispersion is not an issue.

On each night several Lick/IDS standard stars were also observed to transform our observations into the Lick spectral index system (Worthey et al. 1994). To further tie in our observations with population synthesis models, we also observed several stars from two more recent stellar spectral libraries based on the coudé feed spectrograph at the Kitt Peak National Observatory. These libraries are both available at the NOAO website. We note here the more extensive current library, called the Indo-US Library of Coudé Feed Stellar Spectra, which is summarized in Valdes et al. (2004), and available at the `URL: http://www.noao.edu/cflib/`.

3.5. Weather and Instrumental Anomalies

Since the purpose of this database is to provide a homogeneous set of integrated spectra of Galactic globular clusters, we summarize here all aspects of the observations that could generate a departure from a strictly homogeneous dataset. We stress that in all cases these departures are minor and can be appropriately corrected or accounted for.

3.5.1. Bias Level Variations

From frequent monitoring of bias frames, we determined that the bias was subject to large variations during the night. The mean overscan level fluctuated by up to 80 ADU

(hence 80 e^-) during the night and could jump by as much as 10 ADU between consecutive bias frames. In addition, the shape of the overscan varied from one bias frame to the next. On some bias frames, an overall gradient as large as 6 ADU was present across the overscan region, but the trend varied considerably from one frame to the next, and a fifth order polynomial was used to fit the overscan. Fortunately, with only one exception, we found that the overscan-subtracted bias frame is stable, thus a useful overscan-subtracted master bias frame could indeed be constructed from a series of bias exposures, and that master bias is well behaved. The sole exception is the 25 bias frames from the first night. Hence we used the master bias from the second night for the first night as well.

3.5.2. Variable Slit Width in Final Night

As mentioned in §3.1, a glitch in the slit motor occurred approximately midway through the last night of observations. The motor failed while narrowing the slit back to 225 μm after we had widened it to observe a flux standard. After the problem was fixed and the system rebooted, we encountered a zeropoint problem in the slit width; the slit looked visibly wider on the TV monitor for the guider camera. For the next observation, of the globular cluster NGC 6362, the linewidths in the arc spectrum are nearly twice as large as in previous observations. As a result, we narrowed the slit considerably, but ended up with a narrower slit for the rest of that final night than for the first three nights. Indeed the lines in the arc spectra are narrower by $\sim$0.2 pixels in FWHM than for the earlier part of the night. The clusters affected are NGC 6528 (also observed on a previous night), NGC 6553, NGC 6569, NGC 6752, and 47 Tuc. Users of the database should be aware that we have slightly smoothed the spectra of these 5 clusters to give them the same spectral resolution as the rest of the observations. The spectrum of NGC 6362 should only be used for low resolution applications.

3.5.3. Arc Lamp Issues

During the first two nights of the observing run, the rotator mirror that switches between the main field viewer and the HeNeAr arc lamp was unreliable, and required frequent rebooting and reinitialization of the system. After reinitialization, the wavelength zeropoint could shift by several pixels, which is not a problem since an arc lamp exposure was taken along with the object exposure. However, we caution the reader that we do not consider the radial velocity data extracted from our integrated spectra to be reliable. To circumvent the rotator mirror problem, for the third and fourth nights the penray HeNeAr lamp from the

Hydra multi-fiber spectrograph was used as the wavelength calibration source. This lamp does not provide as uniform and extensive coverage as the HeNeAr source for the R-C spectrograph, particularly at the bluer wavelengths. See §4 for a description of how we handled this problem.

3.5.4. Non-Photometric Conditions

Although the weather was mostly good during the four-night observing run, non-photometric conditions were experienced at times during the first and third nights, i.e., 2003 April 24-25 and 2003 April 26-27. During the first night, thin clouds developed during the second half of the night, and appeared to persist until dawn. Thus the exposures of NGC 6121, NGC 6266, NGC 6284, NGC 6342, and NGC 6626 are all marginally affected by thin clouds on that night. On the third night, however, the evening started with thick cirrus, which eventually developed to the point where we were required to shut down for approximately an hour. Thereafter, the sky cleared rapidly, and the conditions were good for the second half of the night. Exposures of five clusters, NGC 1904, NGC 2298, NGC 2808, NGC 5286, and NGC 5904 were taken under quite heavy clouds, with those of NGC 1904, NGC 2808, and NGC 5286 taken under approximately a magnitude of extra extinction. Note that we have at least one additional exposure for each of these five clusters on other nights.

4. Data Reduction

Analysis of the spectra was carried out using the IRAF software package. We generally followed the procedures described in the tutorials "A User's Guide to CCD Reductions with *IRAF*" by P. Massey and "A User's Guide to Reducing Slit Spectra with *IRAF*" by P. Massey, F. Valdes, and J. Barnes, both available at the IRAF website. The first step involved fitting and removing the overscan region and then subtracting off a master bias frame. An overscan-subtracted master bias frame was created for each night from a series of 25 bias frames (taken at the start of the night). The 25 frames were averaged, with a *minmax* rejection of the highest and lowest values, using the *zerocombine* routine in the *ccdred* package. The bias-subtracted frames were then flat-field corrected. A master flat was produced from a sequence of 25 overscan and bias-subtracted dome flat field frames. The individual flats were averaged, and cosmic ray rejection was achieved using the *crreject* parameter in the *flatcombine* task. Then the instrumental and flat field lamp response was normalized along the dispersion direction using the *response* task and the non-uniform illumination along the slit was measured using a twilight sky exposure according to the *illumination* task. All object

and arc frames were then overscan and bias subtracted, flat-field divided, and illumination corrected.

Next we extracted a one-dimensional spectrum from the two-dimensional data frames. This was accomplished using the *apall* task in the *apextract* package. The extraction aperture was selected by examining the slit profile for the cluster, and generally included the core diameter of the cluster. Two important aspects of the extraction are to trace the location of the cluster spectrum as a function of position along the dispersion axis (the *aptrace* routine) and eliminating cosmic rays (CRs) by making a variance-weighted, cleaned extraction that fits the aperture profile at each wavelength (see the *IRAF* slit spectrum tutorial mentioned above for details). For a few clusters (e.g., NGC 2298), with particularly large core radii and/or a jagged profile along the slit produced by discrete bright stars, it proved difficult to successfully trace the slit profile at all wavelengths. In these cases we simply used the trace from a bright star taken on the same night, but with the aperture resized and initially centered according to the cluster itself.

The *apall* procedure produces not only a variance-weighted, cleaned extracted spectrum, but an unweighted, uncleaned extracted spectrum, and a variance spectrum as well. The variance spectrum was calculated with the detector read noise and gain properly accounted for. The variance spectrum for the extracted cluster spectrum was added in quadrature to the variance spectrum for the extracted sky spectrum to produce a total variance for the final sky-subtracted cluster spectrum. The sky-subtracted cluster spectrum was then divided by the variance spectrum to produce a spectrum that gives the S/N ratio at each pixel.

Wavelength calibration was carried out using an arc spectrum taken at the same pointing position as the cluster spectrum, either immediately before or after the cluster and sky background spectra were acquired. At the start of each night a series of 5 arc spectra were taken, and averaged to form a master arc spectrum for that night. The S/N ratio of the master arc is high enough that many faint lines can be fit, thus stabilizing the wavelength fitting, especially at the blue end of the spectrum. A fourth order Legendre polynomial was fit to the master arc, generally producing rms residuals of $\sim$0.12 Å. Then an extraction was made from the arc taken along with a particular cluster spectrum, and the extraction was made with the same trace and aperture parameters as for the cluster. Since the S/N ratio of the single arc spectrum is considerably lower than for the master arc, we then calculated a zero point shift between the cluster arc and the master arc, using the *reidentify* task. The assumption is that variations in the geometric distortion of the spectrograph will be minimal during the night, with only a zero point shift needing consideration. The wavelength zero point did shift significantly during the night, by up to several pixels. However, we have verified that the zero point has been succesfully monitored, since the wavelength of the

[O I]λ5577 night sky line in the dispersion corrected spectra is very stable from one cluster to another. For the last two nights, when the penray lamp from the Hydra spectrograph was utilized (cf., §3.5.3), we used the master arc from the second night as our high S/N reference arc spectrum.

After the dispersion correction was carried out, the final step was to flux calibrate the data using the typically 3 flux standards observed during each night. Given the low number of flux standards observed, along with the fact that the mean extinction data for CTIO were used, and that non-photometric conditions were encountered on some nights (cf., §3.5.4), we consider the flux calibration to be only approximate. The most useful attribute of our spectral library is the relatively high resolution and high S/N, allowing for numerous line indices, which do not depend on an absolute flux calibration, to be defined and used. Note that our observations do not suffer from the usual problem encountered in narrow-slit high-resolution spectroscopy, namely differential atmospheric refraction. Due to the highly extended nature of our clusters, coupled with our trailing over the cluster core, atmospheric dispersion is not a problem. For our flux standard observations, we opened the slit to 10″ width, to ensure that atmospheric dispersion did not harm the flux standards either.

We determined radial velocities from cross-correlation of the library spectra with an integrated spectrum of 47 Tuc obtained in a previous observing run (see Schiavon et al. 2002a for a description), using the *rv.fxcor* IRAF task. We estimated an internal accuracy of ± 9 kms^{-1} for our radial velocity determinations by measuring the central wavelengths of absorption lines in the blue and red ends of the spectra. Finally, these radial velocities were used to bring the 1-D cluster spectra to the restframe.

5. Integrated Spectra of Galactic Globular Clusters

5.1. Format of the Spectral Library

The finalized library of integrated spectra and electronic versions of Tables 1 and 2 are available at `http://www.noao.edu/ggclib/`. For each cluster the final flux-calibrated spectrum is presented in a single FITS file. Another FITS file, in multi-spectrum format, contains auxiliary spectral information which may be useful to some investigators. The multi-spectrum file contains four spectral bands, each one containing wavelength-calibrated, but *not* flux-calibrated, data. The first band contains the variance-weighted CR-cleaned, sky-subtracted spectrum, while the second band contains the unweighted, uncleaned extraction, both produced by the IRAF *apall* task. The third band contains the *apall* extraction of the sky from the separate sky frame, except for the few instances where we extracted the

sky from the ends of the slit. Those exceptions are mentioned in the notes on individual clusters in §6. The fourth band contains the S/N ratio at each pixel in the spectrum. We call the reader's attention for this slight deviation of the IRAF standard, according to which the fourth band of *apall* output files usually contains the variance spectrum, instead of the S/N ratio. We decided to adopt the latter in order to provide the users with a quick visual estimate of the S/N ratio of the spectra at each pixel. As mentioned earlier, the S/N ratio per pixel was obtained by dividing the sky-subtracted cluster spectrum by the quadrature sum of the variance spectra in the cluster and in the sky. Therefore, the variance spectrum can be recovered by taking the ratio between bands 1 and 4 of the auxiliary files. The README file at the website gives further details on the format of the spectral data.

5.2. Examples of the Globular Cluster Spectra

Figures 2a-h display our complete library of integrated spectra of Galactic globular clusters, ordered by increasing [Fe/H]. While the spectral library is clearly intended for work with quantitative spectral indices, we provide here a few qualitative illustrations of the use of these spectra. We begin by showing the effect of HB morphology on the integrated spectra of old stellar populations. In Figure 3 we compare the integrated spectra of the two moderately metal-poor GCs NGC 6723 and NGC 6652. While the two clusters have virtually the same [Fe/H] (Table 1) NGC 6652 is characterized by a red HB morphology, whereas NGC 6723 has a comparable number of blue and red HB stars (Piotto et al. 2002). The impact of the blue HB stars in the integrated spectrum of NGC 6723 can be easily seen by the substantially *stronger* Balmer lines and *weaker* metallic features (see also Schiavon et al. 2004b). Figure 4 shows a similar comparison in a more metal-rich regime. NGC 6441 and NGC 6304 are more metal-rich than the above two clusters by ~ 0.5 dex, which is readily noticeable due to their much stronger metal lines. In NGC 6304, the horizontal branch is made solely of red stars, while in the case of NGC 6441 it is dominated by red stars but contains a sizeable blue extension. The effect of HB stars on the integrated spectrum of NGC 6441 is more subtle than for the metal poor clusters discussed above. While Balmer lines are clearly stronger in the spectrum of NGC 6441, metal lines appear to be only weakly sensitive to the influence of the blue HB stars, their strengths being only slightly weaker in the spectrum of NGC 6441, probably because the horizontal branch of the latter has a dominant red component.

It is well established that the best age indicators for stellar populations use the sensitivity of Balmer lines to the main sequence turnoff temperature (Worthey 1994). Hence one must track any conditions under which anomalous emission lines could lead to an artificial fill-in of the Balmer lines in the integrated spectrum of a cluster. Specifically, clusters at low

galactic latitude can have a foreground weak diffuse H II emission region superimposed on the cluster. An example of this effect is seen in Fig. 5, where the two-dimensional spectrum of NGC 3201 is shown, covering the [O II]λ3727 emission line which extends across the entire slit. The presence of [O II] emission implies that there is emission in the Balmer lines as well. The latter, if not appropriately subtracted, would fill-in the Balmer lines in absorption, making them appear artificially weak and thereby making the cluster appear spuriously old. The identification and removal of any diffuse emission is thus crucial. To further emphasize this point with a second cluster, NGC 6352, which has foreground [O II] emission, we plot in Fig. 6 the background-subtracted spectrum of NGC 6352 (bottom) and the "raw" spectrum before sky subtraction (top). The [O II] 3727 emission is readily seen in the raw spectrum, and is greatly reduced in the subtracted spectrum. (Note that the [O II] 3727 emission is superposed on a pseudo-continuum peak in the line-rich absorption spectrum of NGC 6352, making it difficult to assess the degree of emission contamination without subtracting out the underlying absorption spectrum of the cluster).

For one last example, we take a closer look at the integrated spectrum of the relatively metal-rich globular cluster NGC 6637 (= M69). This cluster contains an emission-line star near the center, as can be seen in Fig. 7, where we show the two-dimensional spectrum of NGC 6637 in the wavelength region covering Hδ and Hγ. Aside from a few random CRs, the localized emission in Hγ and Hδ at one specific location on the slit (where the slit trailed across the emission-line star) is clearly evident. This fact has been previously noted by Rose & Tripicco (1986), who tentatively classified the star as a long-period variable (LPV). In order to further investigate the nature of the emission-line star we extracted its individual spectrum and verified that it contains TiO bands whose strength are consistent with an M2-3 spectral type, so that if the star is a cluster member its classification as a LPV is reliable. Moreover, the strengths of the Balmer lines are consistent with those of emission-line M giants found in the field (e.g. Pereira, Franco & de Araújo 2003). However, we tried to match the position of the emission-line star in the 2D spectrum with the positions of known LPV stars in the cluster (Hartwick & Sandage 1968, Rosino 1962), without success. We also speculated whether the emission line star could perhaps be a symbiotic star or a foregroud flaring M dwarf. However, the spectra of symbiotic stars are characterized by the presence of strong HeI and [OIII] lines which are absent in our spectrum (e.g. Luna & Costa 2005, Warner 1995). The same applies to the case of flare M dwarfs, whose spectra are characterized by the presence of the CaII H and K lines in emission (e.g. Petit 1987), which are also not seen in the spectrum of the emission-line star in NGC 6637. Therefore, we suggest that this emission-line star is *likely* to be a LPV member of the cluster.

Given the high luminosity of stars at the giant branch tip, the strong Balmer emission lines due only to this star can significantly affect the integrated spectrum of the cluster. This

is shown in Figure 8, where the variance-weighted "optimum" extraction of the integrated spectrum and the unweighted extraction are both plotted. Note the major discrepancy in the strengths of Hδ and Hγ between the two extractions. The difference is due to the fact that the variance-weighted extraction identifies and removes the bright emission spots in the two-dimensional spectrum, just as it does for CRs. While the identification of the emission lines with CRs is incorrect, they certainly have that appearance in Figure 7, and their removal from the variance-weighted extraction fortunately avoids the otherwise catastrophic influence of the LPV emission on the integrated Balmer lines of the cluster.

The example above raises two important issues. Firstly, under special circumstances, the influence of a single star can clearly affect the integrated light of the cluster, even when the entire core diameter is covered. Thus it is important to check for any particularly bright object along the slit. Secondly, our exercise identified a case where the variance-weighted extraction procedure rejected the localized emission lines from the LPV as CRs, which was fortunate, but we can imagine other less benign situations. Essentially, any bright star in the cluster with a very different spectrum from the rest of the cluster is a target for removal by the variance-weighted extraction. For most clusters, this is not an issue, because the light profile along the slit is fairly smooth. However, for a few of the less concentrated clusters, the choice of spectral extraction technique can have an impact on the final results. For this reason, in the data products we have included both variance-weighted and unweighted extractions in the multi-spectrum FITS file for each cluster, as was discussed above. Thus one can directly search for anomalies created by the particular extraction technique. Note that the unweighted extraction has *not* been cleaned of CRs.

6. Notes on Individual Clusters

In this section we provide information on individual clusters.

NGC 104 = 47 Tuc: 47 Tuc is so bright that no separate sky exposure was taken. This is one of the clusters observed during the last night when the slit width was slightly narrower than for the other observations. We have smoothed the final spectrum of this cluster to match the spectral resolution of the other clusters.

NGC 1904: It was difficult to obtain a successful aperture trace for this cluster, due to the presence of a very red star that traversed the slit right at the center of the cluster. However, by adjusting the step size of the aperture trace, a successful trace was carried out.

NGC 2298: NGC 2298 could not be successfully traced for aperture extraction, due to a large number of discrete bright stars crossing the slit, and creating a jagged slit profile.

Consequently, we used the aperture trace from a stellar spectrum taken on the same night, but recentered the aperture and resized it. There are two spectra of this cluster, taken on different nights, with very slightly different aperture extractions.

NGC 2808: Two exposures were taken, heavy clouds compromise the second one. We used slightly different aperture extractions for the two exposures.

NGC 3201: NGC 3201 is a cluster with a particularly large core diameter. It is somewhat difficult to determine the cluster center. We obtained spectra for the cluster on both UT 25-APR-2003 and UT 26-APR-2003. There is strong [OII]λ3727 emission evident across the entire slit in both cluster exposures and the two sky background regions scanned (the sky background regions scanned were different on the two nights, as is recorded in Table 2. An extremely bright star crossed the slit during the sky background trail for the exposure on UT 25-APR-2003. Consequently, we decreased the extracted aperture on the sky background frame to $\pm$55 pixels ($\pm 55''$), to avoid the contaminated location on the slit. We then renormalized the sky counts to match the $\pm$85 pixel extraction on the cluster. This problem did not occur for the exposure on UT 26-APR-2003, for which we scanned a different sky background region. Note that the [OII]λ3727 emission subtraction appears to come out cleaner for the UT 26-APR-2003 exposure.

NGC 5286: There is no arc for NGC 5286 on the night of UT 2003-04-27, so we used the arc for NGC 2808, and made a zeropoint correction using night sky lines.

NGC 5904: NGC 5904 could not be successfully traced at all, maybe a result of too many discrete stars crossing the slit with different SED's. So we used the trace from the star HD102574, but recentered the aperture and resized it.

NGC 5927: NGC 5927 was difficult to trace, so used trace from the star HD76151, but recentered the aperture and resized it.

NGC 5986: The trail across NGC 5986 intersected a very bright star. We did not choose to eliminate the bright star from our aperture extraction.

NGC 6171: There is extended [OII]λ3727 emission across this spatially extended cluster. To obtain a successful aperture trace for the cluster it was necessary to center the extracted aperture on the brightest peak on the slit profile rather than on the average center of the light distribution.

NGC 6284: NGC 6284 is so centrally concentrated that we defined two apertures. The first aperture contains the FWHM of the slit profile, while the second contains a substantially wider region along the slit.

NGC 6342: NGC 6342 is so centrally concentrated that we defined two apertures. The first aperture contains the FWHM of the slit profile, while the second contains a substantially wider region along the slit.

NGC 6544: NGC 6544 has an extremely peaked light profile along the slit that is offset by several arcseconds from the centroid of the fainter light levels. We used the peak in the light profile for the center of the extracted aperture, but used asymmetric limits for the aperture.

NGC 6352: NGC 6352 has emission at [OII]λ3727. Sky subtraction in [OII] emission came out better when the background was subtracted from the ends of the slit rather than from the separate sky background exposure. The background in the separate frame was further compromised by several bright stars that went through the slit in the 5′trail. Hence we used the ends of the slit for sky subtraction in this case.

NGC 6362: The spectrun for this cluster has degraded resolution, due to the problem of the slit width control described in §3.5.2.

NGC 6441: NGC 6441 is so centrally concentrated that we defined two apertures. The first aperture contains the FWHM of the slit profile, while the second contains a substantially wider region along the slit.

NGC 6528: For the 28-APR-2004 observations of NGC 6528 inaccuracy in the tracking led to the 15 minute trail not covering the anticipated 9″. As a result we took a second 15 minute exposure, which picked up the trail where it ended in the first exposure. The counts in the second exposure are very similar to those int he first exposure. We have maintained these as two separate observations (NGC6528b*.fits and NGC6528c*.fits) because they are taken from different parts of the cluster. In addition, NGC 6528 is so centrally concentrated that we defined two apertures. The first aperture contains the FWHM of the slit profile, while the second contains a substantially wider region along the slit. Finally. we have smoothed the final spectra of this cluster taken on 28-APR-2004 to match the spectral resolution of the other clusters.

NGC 6553: This is perhaps the most problematic cluster in the sample. It is in a high background region of the bulge, with variable obscuration and variable [OII] emission. In addition, NGC 6553 is not a centrally concentrated cluster. Consequently, it was a difficult cluster to trace, so we used the trace from a star, but with redefined apertures. We found that the [OII] and Balmer emission in the background is stronger in the separate sky exposure than at the ends of the slit for the cluster exposure. Consequently, we used the ends of the slit for background subtraction. In addition, there is a bright blue foreground star that traversed the slit during the cluster exposure. This star is bright enough to make an appreciable impact in strengthening the Balmer lines in the integrated cluster spectrum. Hence we

separately extracted the slit position corrsponding tot he bright star and subtracted that off. Nevertheless, even when the bright star contributioin is removed, the relative depths of Ca II H and K lines indicates a contribution from hot stars to the integrated spectrum of this cluster. We believe this reflects the contribution of blue straggler stars that are seen in the color-magnitude diagram of the cluster.

NGC 6569: NGC 6569 is one of the clusters observed during the last night when the slit width was slightly narrower than for the other observations. We have smoothed the final spectrum of this cluster to match the spectral resolution of the other clusters.

NGC 6624: NGC 6624 is so centrally concentrated that we defined two apertures. The first aperture contains the FWHM of the slit profile, while the second contains a substantially wider region along the slit.

NGC 6637: NGC 6637 has a long period variable in emission in the cluster core. The cleaned, variance-weighted extraction is unaffected by this (the LPV Balmer line emission is confused with cosmic rays and cleaned out), but the raw counts extraction has the Balmer lines seriously weakened by the emission in the star. See §5.2 for further details.

NGC 6652: For this cluster either the discrete digitization of the trail rate or inaccuracy in the tracking led to the 15 minute trail not covering the aniticipated 9″. As a result we took a second 15 minute exposure, which picked up the trail where it ended in the first exposure. The counts in the second exposure are ∼30% higher than in the first exposure. We have maintained these as two separate observations because they are taken from different parts of the cluster.

NGC 6723: We took a 10 minute exposure on the cluster and only a 5 minute sky exposure, thus doubled the sky counts before subtracting them from the cluster.

NGC 6752: NGC 6752 is one of the clusters observed during the last night when the slit width was slightly narrower than for the other observations. We have smoothed the final spectrum of this cluster to match the spectral resolution of the other clusters.

NGC 7078: NGC 7078 is so centrally concentrated that we defined two apertures. The first aperture contains the FWHM of the slit profile, while the second contains a substantially wider region along the slit.

NGC 7089: We used sky from the ends of the slit, rather than from the subsequent sky exposure, because the sky background was starting to brighten considerably with approaching dawn.

7. Summary

We have collected a new library of integrated spectra of Galactic globular clusters, with high S/N and moderately high resolution. We envisage at least two chief applications for this new dataset. Firstly, it should serve as a reliable database for local, well-known stellar populations, against which the observations of remote, unresolved, systems can be contrasted. Secondly, this library can be used to verify the accuracy and reliability of the predictions of stellar population synthesis models. For both purposes, it is crucial that the fundamental parameters of the clusters that make up the library be well known, and for that reason we selected our targets amongst those with best color-magnitude and metal-abundance data. Further applications aiming at a detailed calibration of stellar population synthesis models are currently under way. The spectral library is publicly available in electronic format from the National Optical Astronomical Observatory website.

We thank the referee, Guy Worthey, for suggestions that improved this paper. R.P.S. acknowledges financial support from NSF grant AST 00-71198 to the University of California-Santa Cruz, and from HST Treasury Program grant GO-09455.05-A to the University of Virginia. S.C. and L.A.M. are grateful to the NSERC for financial support through a Discovery grant. This research was partially supported by NSF grant AST-0406443 to the University of North Carolina-Chapel Hill.

REFERENCES

Beasley, M.A., Hoyle, F. & Sharples, R.M. 2002, MNRAS, 336, 168

Bica, E. & Alloin, D. 1986, A&A, 162, 21

Borkova, T. V., & Marsakov, V. A. 2000, Astron. Rep., 44, 665

Brocato, E., Castellani, V., Raimondo, G. & Walker, A.R. 1999, ApJ, 527, 230

Bruzual, G. & Charlot, S. 2003, MNRAS, 344, 1000

Bruzual, G., Barbuy, B., Ortolani, S., Bica, E., Cuisinier, F., Lejeune, T. & Schiavon, R.P. 1997, AJ, 114, 1531

Burstein, D., Faber, S.M., Gaskell, C.M. & Krumm, N. 1984, ApJ, 287, 586

Carretta, E. & Gratton, R.G. 1997, A&AS, 121, 95

Cohen, J.G., Blakeslee, J.P. & Ryzhov, A. 1998, ApJ, 496, 808

Covino, S., Galletti, S. & Pasinetti, L.E. 1995, A&A, 303, 79

Djorgovski, S. 1993, ASP Conference Series, 50, 373

Djorgovski, S. & Meylan, G. 1993, ASP Conference Series, 50, 325

Faber, S.M. 1973, ApJ, 179, 731

Feltzing, S. & Johnson, R.A. 2002, A&A, 385, 67

Fullton, L.K., Carney, B.W., Olszewski, E.W., Zinn, R., Demarque, P., Janes, K.A., Da Costa, G.S. & Seitzer, P. 1995, AJ, 110, 652

Gibson, B.K., Madgwick, D.S., Jones, L.A., Da Costa, G. & Norris, J.E. 1999, AJ, 118, 1268

Hargis, J.R., Sandquist, E.L. & Bolte, M. 2004, ApJ, 608, 243

Harris, W.E. 1996, AJ, 112, 1487

Hartwick, F.D.A. & Sandage, A. 1968, ApJ, 153, 715

Howell, J.H., Guhathakurta, P. & Gilliland, R.L. 2000, PASP, 112, 1200

Janes, K.A. & Heasley, J.N. 1991, AJ, 101, 2097

Kraft, R.P. & Ivans, I.I. 2003, PASP, 115, 143

Kanatas, I., Griffiths, W.K., Dickens, R.J. & Penny, A.J. 1995, AJ, 272, 265

Le Borgne, D., Rocca-Volmerange, B., Prugniel, P., Lançon, A., Fioc, M. & Soubiran, C. 2004, A&A, 425, 881

Lee, Y.-W., Demarque, P. & Zinn, R. 1994, ApJ, 423, 248

Luna, G.J.M. & Costa, R.D.D. 2005, A&A, in press, astro-ph/0502308

Maraston, C., Greggio, L., Renzini, A., Ortolani, S., Saglia, R.P., Puzia, T.H. & Kissler-Patig, M. 2003, A&A, 400, 823

Markov, H.S., Spassova, N.M. & Baev, P.V. 2001, MNRAS, 326, 102

Momany, Y., Piotto, G., Recio-Blanco, A., Bedin, L.R., Cassisi, S. & Bono, G. 2002, ApJ, 576, L65

Momany, Y., Ortolani, S., Held, E.V., Barbuy, B., Bica, E., Renzini, A., Bedin, L.R., Rich, R.M. & Marconi, G. 2003, A&A, 402, 607

Ortolani, S., Momany, Y., Barbuy, B., Bica, E., Catelan, M. 2000, A&A, 362, 953

Ortolani, S., Bica, E. & Barbuy, B. 2001, A&A, 374, 564

Pereira, C.B., Franco, C.S. & de Araújo, F.X. 2003, A&A, 397, 927

Peterson, C.J. 1993, ASP Conference Series, 50, 337

Petit, M. 1987, Variable Stars (New York: John Wiley & Sons)

Piotto, G. et al. 2002, A&A, 391, 945

Proctor, R.N., Forbes, D.A. & Beasley, M.A. 2004, MNRAS, 355, 1327

Pulone, L., De Marchi, G., Covino, S. & Paresce, F. 2003, A&A, 399, 121

Puzia, T.H., Saglia, R.P., Kissler-Patig, M., Maraston, C., Greggio, L., Renzini, A. & Ortolani, S. 2002, A&A, 395, 45

Rose, J.A. 1985, AJ, 90, 1927

Rose, J.A. 1994, AJ, 107, 206

Rose, J.A. & Tripicco, M.J. 1986, AJ, 92, 610

Rosenberg, A., Piotto, G., Saviane, I. & Aparicio, A. 2000a, A&AS, 144, 5

Rosenberg, A., Aparicio, A., Saviane, I. & Piotto, G. 2000b, A&AS, 145, 451

Rosino, L. 1962, Mem.Soc.Astron.It. 33, 351

Samus, N., Ipatov, A., Smirnov, O., Kravtsov, V., Alcaino, G., Liller, W. & Alvarado, F. 1995, A&A, 112, 439

Sandquist, E., Bolte, M., Stetson, P.B. & Hesser, J.E. 1996, ApJ, 470, 910

Schiavon, R.P. & Barbuy, B. 1999, ApJ, 510, 934

Schiavon, R.P., Faber, S.M., Castilho, B.V. & Rose, J.A. 2002a, ApJ, 580, 850

Schiavon, R.P., Faber, S.M., Rose, J.A. & Castilho, B.V. 2002b, ApJ, 580, 873

Schiavon, R.P., Caldwell, N. & Rose, J.A. 2004a, AJ, 127, 1513

Schiavon, R.P., Rose, J.A., Courteau, S., & MacArthur, L. 2004b, ApJ, 608, L33

Thomas, D., Maraston, C. & Bender, R. 2003, MNRAS, 339, 897

Valdes, F., Gupta, R., Rose, J.A., Singh, H.P. & Bell, D.J. 2004, ApJS, 152, 251

Vazdekis, A. 1999, ApJ, 513, 224

Vazdekis, A., Salaris, M., Arimoto, N. & Rose, J.A. 2001, ApJ, 549, 274

von Braun, K. & Mateo, M. 2001, AJ, 121, 1522

von Braun, K., Mateo, M., Chiboucas, K., Athey, A. & Hurley-Keller, D. 2002, AJ, 124, 2067

Warner B. 1995, Cataclysmic Variable Stars (New York: Cambridge Univ. Press)

Worthey, G. 1994, ApJS, 95, 107

Worthey, G., Faber, S.M., González, J.J. & Burstein, D. 1994, ApJS, 94, 687

Zinn, R. & West, M.J. 1984, ApJS, 55, 45

Zoccali, M., Renzini, A., Ortolani, S., Bica, E. & Barbuy, B. 2001, AJ, 121, 2638

Table 1. Sample Clusters

NGC (1)	Other (2)	l (3)	b (4)	R_{GC} (5)	r_c (6)	c (7)	$E(B-V)$ (8)	[Fe/H] (9)	$\frac{(B-R)}{(B+V+R)}$ (10)	CMD Ref. (11)
104	47 Tuc	305.90	-44.89	7.4	0.40	2.03	0.04	-0.70[b]	-0.99	1,2,12
1851		244.51	-35.04	16.7	0.06	2.32	0.02	-1.21[d]	-0.36	1,2
1904	M 79	227.23	-29.35	18.8	0.16	1.72	0.01	-1.55[d]	-0.89	1,2
2298[a]		245.63	-16.01	15.1	0.34	1.28	0.15	-1.97[b]	0.93	2
2808		282.19	-11.25	11.0	0.26	1.77	0.23	-1.29[d]	-0.49	1,2
3201		277.23	8.64	9.0	1.43	1.30	0.21	-1.56[b]	0.08	1,2,14
5286[a]		311.61	10.57	7.2	0.29	1.46	0.24	-1.51[e]	0.80	4
5904	M 5	3.86	46.80	6.2	0.42	1.83	0.03	-1.26[b]	0.31	1,3,13,21
5927		326.60	4.86	4.5	0.42	1.60	0.45	-0.64[c]	-1.00	1,2
5946		327.58	4.19	7.4	0.08	2.50	0.54	-1.54[e]	B[f]	1
5986		337.02	13.27	4.8	0.63	1.22	0.27	-1.53[d]	0.97	1,2,17
6121[a]	M 4	350.97	15.97	6.2	0.83	1.59	0.40	-1.15[b]	-0.06	2,5
6171	M 107	3.37	23.01	3.3	0.54	1.51	0.33	-1.13[d]	-0.73	1,2
6218	M 12	15.72	26.31	4.5	0.72	1.39	0.19	-1.32[d]	0.97	1,3,15,16
6235		358.92	13.52	2.9	0.13	1.33	0.36	-1.36[d]	0.89	1
6254[a]	M 10	15.14	23.08	4.7	0.86	1.40	0.28	-1.51[b]	0.98	3,15
6266	M 62	353.58	7.32	1.7	0.18	1.70	0.47	-1.20[d]	0.32	1,2
6284		358.35	9.94	6.9	0.07	2.50	0.28	-1.27[e]	B[f]	1
6304		355.83	5.38	2.1	0.21	1.80	0.52	-0.66[c]	-1.00	1,2
6316		357.18	5.76	3.2	0.17	1.55	0.51	-0.90[e]	-1.00	1
6333[a]	M 9	5.54	10.71	1.7	0.58	1.15	0.35	-1.65[e]	0.87	6
6342		4.90	9.73	1.7	0.05	2.50	0.46	-1.01[e]	-1.00	1
6352[a]		341.42	-7.17	3.1	0.83	1.10	0.19	-0.70[c]	-1.00	2,7,8
6356		6.72	10.22	7.6	0.23	1.54	0.28	-0.74[e]	-1.00	1
6362		325.55	-17.57	5.3	1.32	1.10	0.08	-1.17[d]	-0.58	1,2,18
6388		345.56	-6.74	4.4	0.12	1.70	0.40	-0.68[e]	I[f]	1
6441		353.53	-5.01	3.5	0.11	1.85	0.44	-0.65[e]	I[f]	1
6522		1.02	-3.93	0.6	0.05	2.50	0.48	-1.39[d]	0.71	1
6528[a]		1.14	-4.17	1.5	0.09	2.29	0.62	-0.10[d]	-1.00	9,19
6544		5.84	-2.20	5.4	0.05	1.63	0.73	-1.38[d]	1.00	1,2
6553[a]		5.25	-3.02	4.6	0.55	1.17	0.80	-0.20[d]	-1.00	10
6569		0.48	-6.68	1.2	0.37	1.27	0.56	-1.08[e]	MR[f]	1,20
6624		2.79	-7.91	1.2	0.06	2.50	0.28	-0.70[c]	-1.00	1
6626[a]	M 28	7.80	-5.58	2.4	0.24	1.67	0.38	-1.21[d]	0.90	2
6637	M 69	1.72	-10.27	1.6	0.34	1.39	0.16	-0.78[c]	-1.00	1,2
6638		7.90	-7.15	1.6	0.26	1.40	0.40	-1.08[d]	-0.30	1,2
6652		1.53	-11.38	2.4	0.07	1.80	0.09	-1.10[e]	-1.00	1
6723		0.07	-17.30	2.6	0.94	1.05	0.05	-1.14[d]	-0.08	1,2
6752[a]		336.50	-25.63	5.1	0.17	2.50	0.04	-1.57[b]	1.00	2,11
7089	M 2	53.38	-35.78	10.4	0.34	1.80	0.06	-1.49[e]	0.96	1

[a]Galactic coordinates, Galactocentric distances and reddenings come from Djorgovski & Meylan (1993), Djorgovski (1993), and Peterson (1993)

[b][Fe/H] from Kraft & Ivans (2003); [c][Fe/H] from Carretta & Gratton (1997); [d][Fe/H] from Carretta & Gratton (1997); corrected by -0.18 dex (see text); [e][Fe/H] from Schiavon et al. (2005, in preparation)

[f]B: blue HB, no clear red HB stars seen; I: intermediate type HB, with pronounced red clump plus an extended blue tail; MR: mostly red, with a sparse blue component

Note. — References to color-magnitude diagrams in the literature: 1) Piotto et al. (2002); 2) Rosenberg et al. (2000a); 3) Rosenberg et al. (2000b); 4) Samus et al. (1995); 5) Kanatas et al. (1995); 6) Janes & Heasley (1991); 7) Pulone et al. (2003); 8) Fullton et al. (1995); 9) Feltzing & Johnson (2002); 10) Zoccali et al. (2001); 11) Momany et al. (2002); 12) Howell et al. (2000), 13) Markov et al. (2001); 14) von Braun & Mateo (2001); 15) von Braun et al. (2002); 16) Hargis et al. (2004); 17) Ortolani et al. (2000); 18) Brocato et al. (1999); 19) Momany et al. (2003); 20) Ortolani et al. (2001); 21) Sandquist et al. (1996).

Table 2. Journal of Observations for Galactic Globular Clusters

(1)	(2)	(3)	(4)	(5)	(6)	(7)	(8)	(9)
NGC 104	2003-04-28	5	E-W	48″	···	···	···	±25″
NGC 1851	2003-04-25	5	N-S	9″	5	20′W	···	±9″
NGC 1904	2003-04-26	15	E-W	20″	15	15′E	···	±10″
NGC 1904	2003-04-27	15	E-W	20″	15	15′E	···	±14″
NGC 2298	2003-04-27	15	E-W	36″	15	15′E	···	-24″, +20″
NGC 2298	2003-04-28	15	E-W	36″	15	15′E	···	±20
NGC 2808	2003-04-25	10	E-W	30″	5	15′E	···	±20
NGC 2808	2003-04-27	10	E-W	30″	10	15′W	5′	-17″, +15″
NGC 3201	2003-04-25	15	N-S	170″	15	12′W	5′	±85″
NGC 3201	2003-04-26	15	N-S	170″	15	12′N	5′	±85″
NGC 5286	2003-04-25	10	N-S	36″	10	12′N	5′	±20″
NGC 5286	2003-04-27	10	E-W	36″	10	12′W	5′	±20″
NGC 5286	2003-04-28	15	E-W	36″	15	12′W	5′	-20″, +23″
NGC 5904	2003-04-27	15	E-W	54″	15	20′W	5′	-27″, +30″
NGC 5904	2003-04-28	15	E-W	45″	15	20′N	5′	-27″, +30″
NGC 5927	2003-04-25	15	N-S	50″	15	20′W	10′	±29
NGC 5927	2003-04-25	15	N-S	50″	15	15′E	10′	±29
NGC 5927	2003-04-28	15	E-W	46″	15	15′E	10′	±25
NGC 5946	2003-04-26	15	N-S	10″	15	10′W	10′	-6″, +7″
NGC 5986	2003-04-25	15	N-S	76″	15	12′N	5′	-32″, +42″
NGC 6121	2003-04-25	15	N-S	100″	15	14′S, 14′W	10′	±50″
NGC 6171	2003-04-26	15	N-S	64″	15	11′N, 11′W	10′	-32″, +36″
NGC 6171	2003-04-26	15	N-S	64″	15	10′S	10′	-32″, +37″
NGC 6218	2003-04-27	15	E-W	90″	15	20′W	10′	±45″
NGC 6235	2003-04-28	15	E-W	45″	15	20′N	10′	±25″
NGC 6254	2003-04-27	15	E-W	108″	15	15′N	10′	±54″
NGC 6266	2003-04-25	15	N-S	22″	15	15′N	5′	-12″, +16″
NGC 6284	2003-04-25	15	N-S	9″	15	15′N	5′	-6″, +7″
···	···	···	···	···	···	···	···	±14″
NGC 6304	2003-04-26	15	N-S	26″	15	10′N	5′	±17″
NGC 6316	2003-04-26	15	N-S	20″	15	10′E	5′	-10″, +11″
NGC 6316	2003-04-28	15	E-W	18″	15	10′W	5′	-14″, +11″
NGC 6333	2003-04-26	15	N-S	70″	15	15′E	5′	±35″
NGC 6342	2003-04-25	10	N-S	12″	10	10′S	5′	±4″
···	···	···	···	···	···	···	···	±10″
NGC 6352	2003-04-27	15	E-W	99″	···	···	···	±50″
NGC 6356	2003-04-26	15	N-S	28″	15	15′E	5′	±22″

Table 2—Continued

(1)	(2)	(3)	(4)	(5)	(6)	(7)	(8)	(9)
NGC 6362	2003-04-28	15	E-W	160″	15	15′W	5′	±80″
NGC 6388	2003-04-26	10	N-S	18″	10	10′E	5′	±10″
NGC 6441	2003-04-26	10	N-S	12″	10	10′E	5′	±10″
...	...	...	...	...	...	...	...	±18″
NGC 6522	2003-04-26	15	N-S	9″	15	8′S	5′	±9″
NGC 6528	2003-04-27	15	E-W	9″	15	8′N	5′	±8″
...	...	...	...	...	...	...	...	±15″
NGC 6528[a]	2003-04-28	15	E-W	5″	15	15′W	5′	±7″
...	...	...	...	...	...	...	...	±14″
NGC 6544	2003-04-26	15	N-S	18″	15	15′E	10′	-12″, +6″
NGC 6553	2003-04-28	15	E-W	64″	15	...	...	±35″
NGC 6569	2003-04-28	15	E-W	45″	15	8′W, 8′S	10′	±25″
NGC 6624	2003-04-27	15	E-W	9″	15	15′S	5′	-7″, +5″
...	...	...	...	...	...	...	...	±11″
NGC 6626	2003-04-25	10	N-S	28″	10	15′S	5′	±16″
NGC 6637	2003-04-27	15	E-W	36″	15	15′N	10′	±20″
NGC 6638	2003-04-27	15	E-W	27″	15	15′N	5′	±15″
NGC 6652	2003-04-27	15	E-W	9″	15	12′W	5′	±7″
NGC 6723	2003-04-27	10	E-W	108″	5	12′W	5′	±54″
NGC 6752	2003-04-28	5	E-W	18″	5	12′W	...	-13″ , +11″
NGC 7078	2003-04-26	5	N-S	9″	...	...	...	±5″
...	...	...	...	...	...	...	...	±20″
NGC 7089	2003-04-28	5	E-W	36″	...	...	...	... ±22″

[a]As discussed in the Notes on this cluster, there were two consecutive exposures made for NGC 6528 on this night, both with the same two aperture sizes.

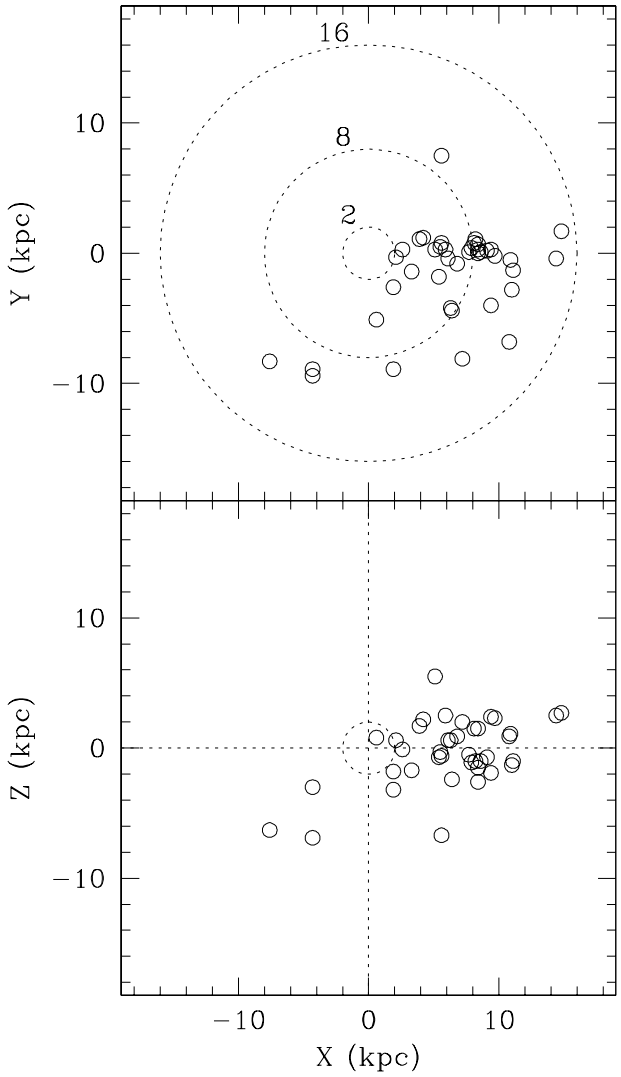

Fig. 1.— Spatial distribution of the sample clusters.

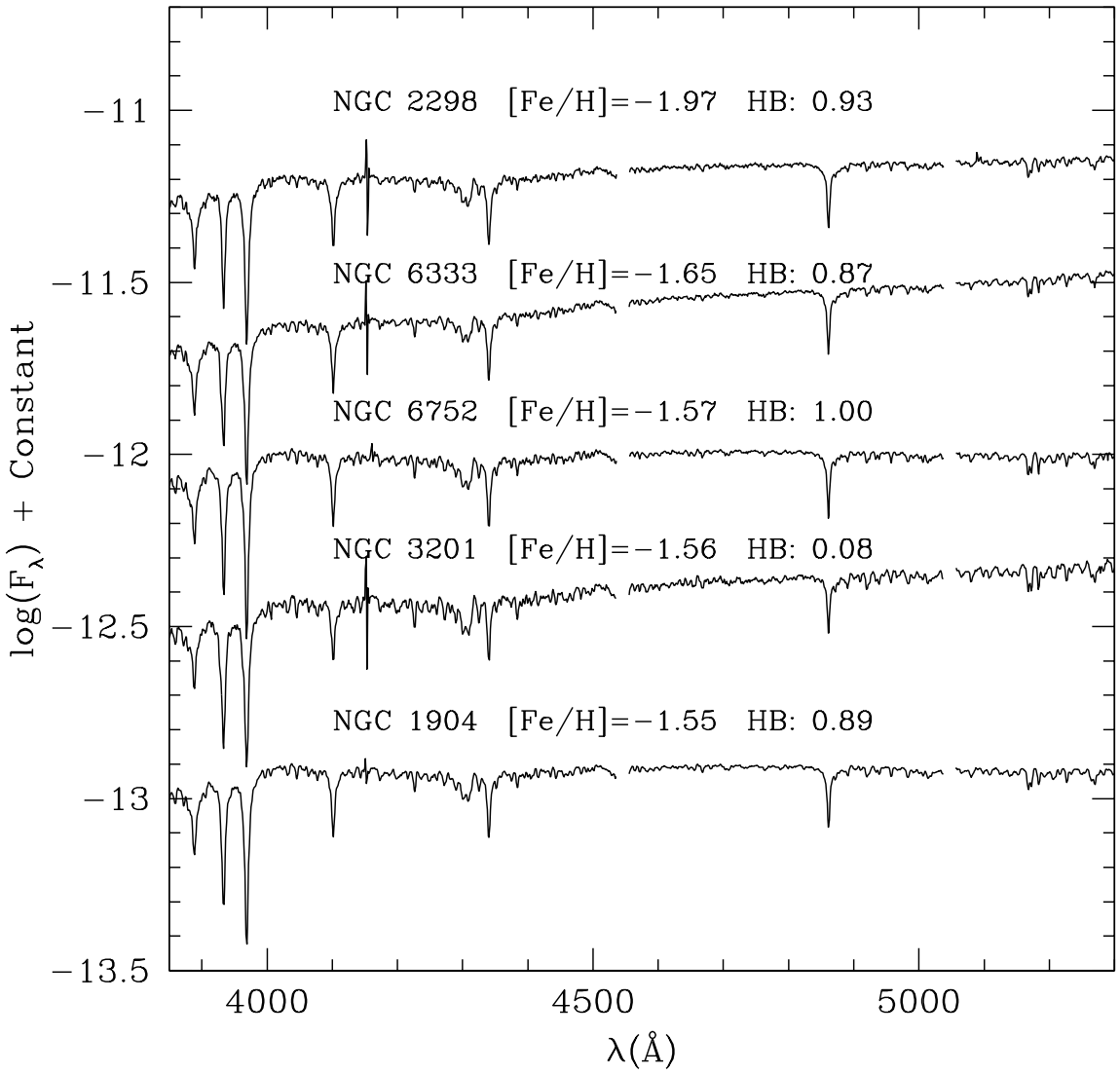

Fig. 2.— a. A segment of the final reduced integrated cluster spectra, in order of increasing metallicity. For clarity, pixels with very deviant fluxes due either to CCD defects or to poorly subtracted sky emission lines were blanked out in this Figure, but preserved in the publicly available electronic library spectra. The spike present in most spectra at ~ 4150 Å is due to a CCD defect.

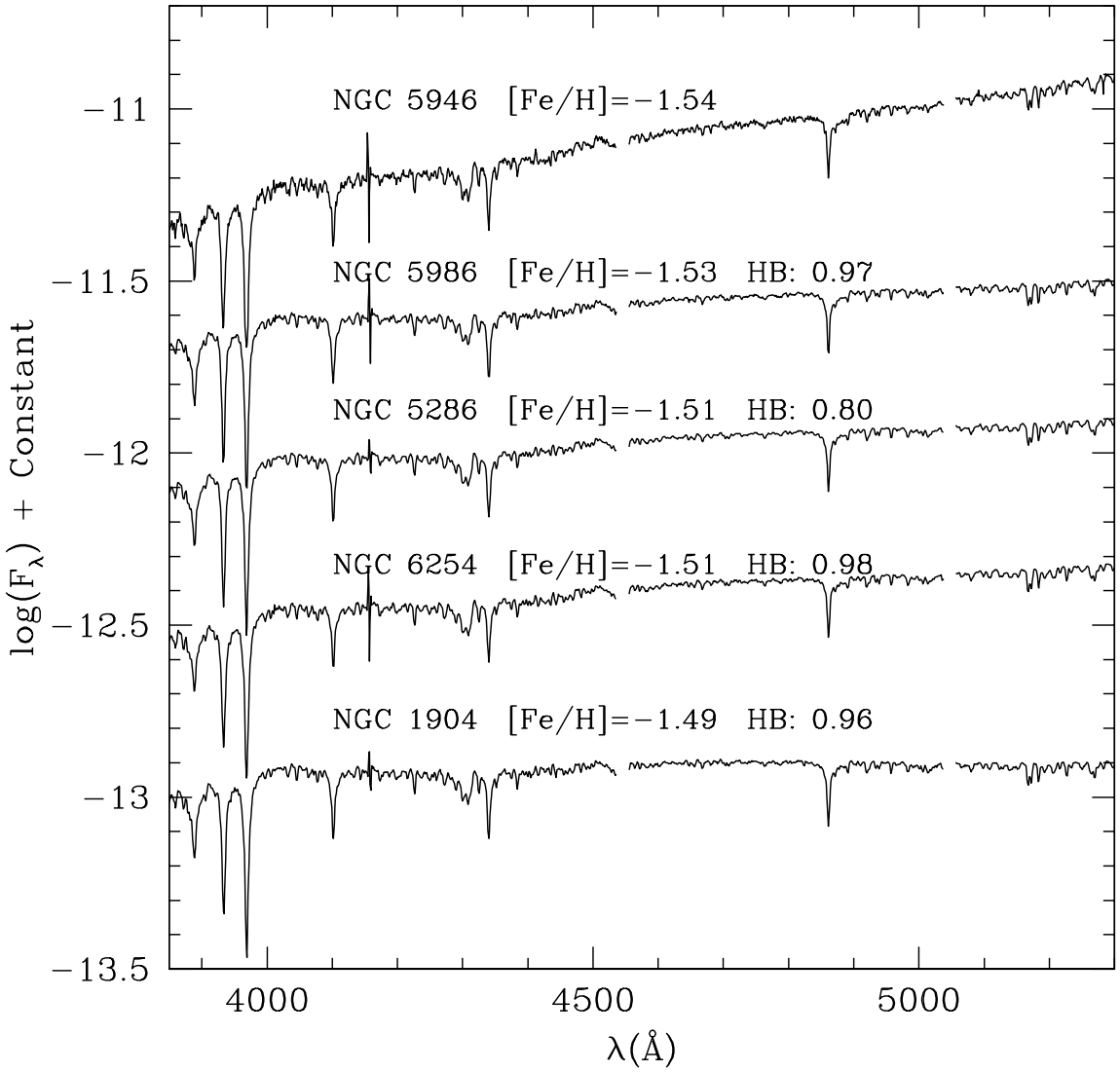
NGC 5946 [Fe/H]=−1.54
NGC 5986 [Fe/H]=−1.53 HB: 0.97
NGC 5286 [Fe/H]=−1.51 HB: 0.80
NGC 6254 [Fe/H]=−1.51 HB: 0.98
NGC 1904 [Fe/H]=−1.49 HB: 0.96
−11
−11.5
−12
−12.5
−13
−13.5
log(F_λ) + Constant
4000
4500
5000
λ(Å)

Fig. 2.— b. Cont.

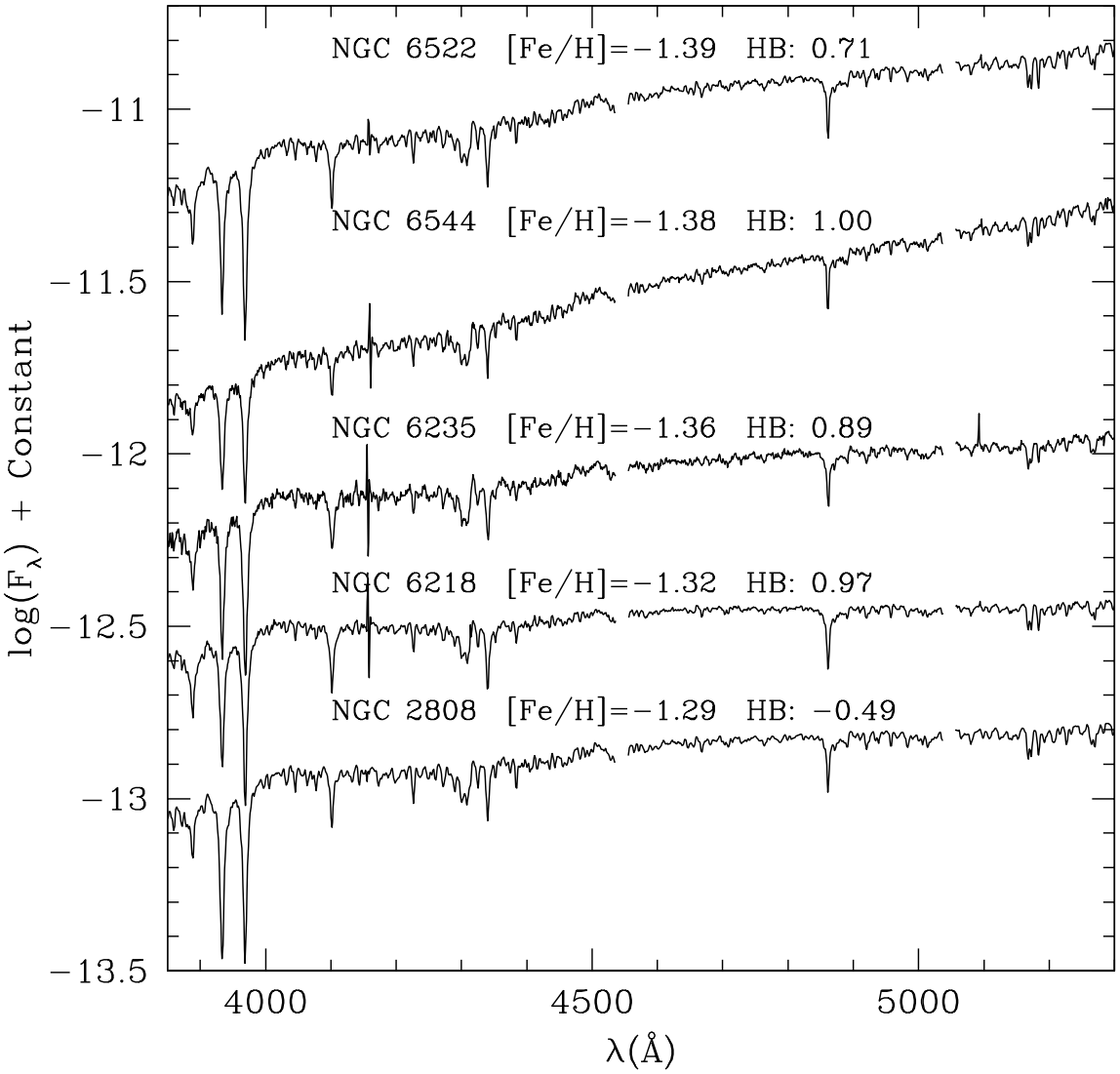
NGC 6522 [Fe/H]=−1.39 HB: 0.71
NGC 6544 [Fe/H]=−1.38 HB: 1.00
NGC 6235 [Fe/H]=−1.36 HB: 0.89
NGC 6218 [Fe/H]=−1.32 HB: 0.97
NGC 2808 [Fe/H]=−1.29 HB: −0.49
−11
−11.5
−12
−12.5
−13
−13.5
log(F_λ) + Constant
4000
4500
5000
λ(Å)

Fig. 2.— c. Cont.

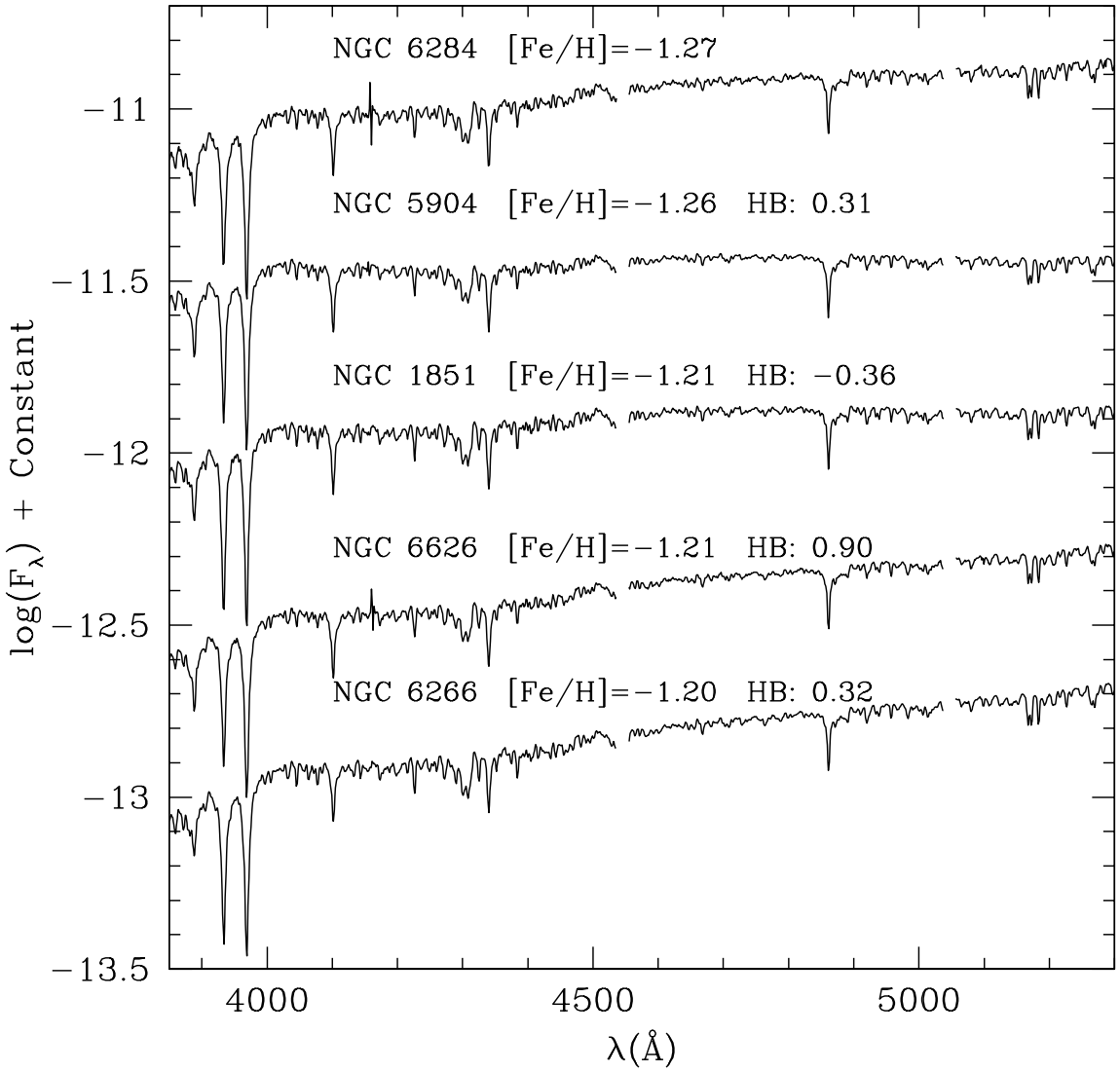
NGC 6284 [Fe/H]=−1.27
NGC 5904 [Fe/H]=−1.26 HB: 0.31
NGC 1851 [Fe/H]=−1.21 HB: −0.36
NGC 6626 [Fe/H]=−1.21 HB: 0.90
NGC 6266 [Fe/H]=−1.20 HB: 0.32
−11
−11.5
−12
−12.5
−13
−13.5
log(F_λ) + Constant
4000
4500
5000
λ(Å)

Fig. 2.— d. Cont.

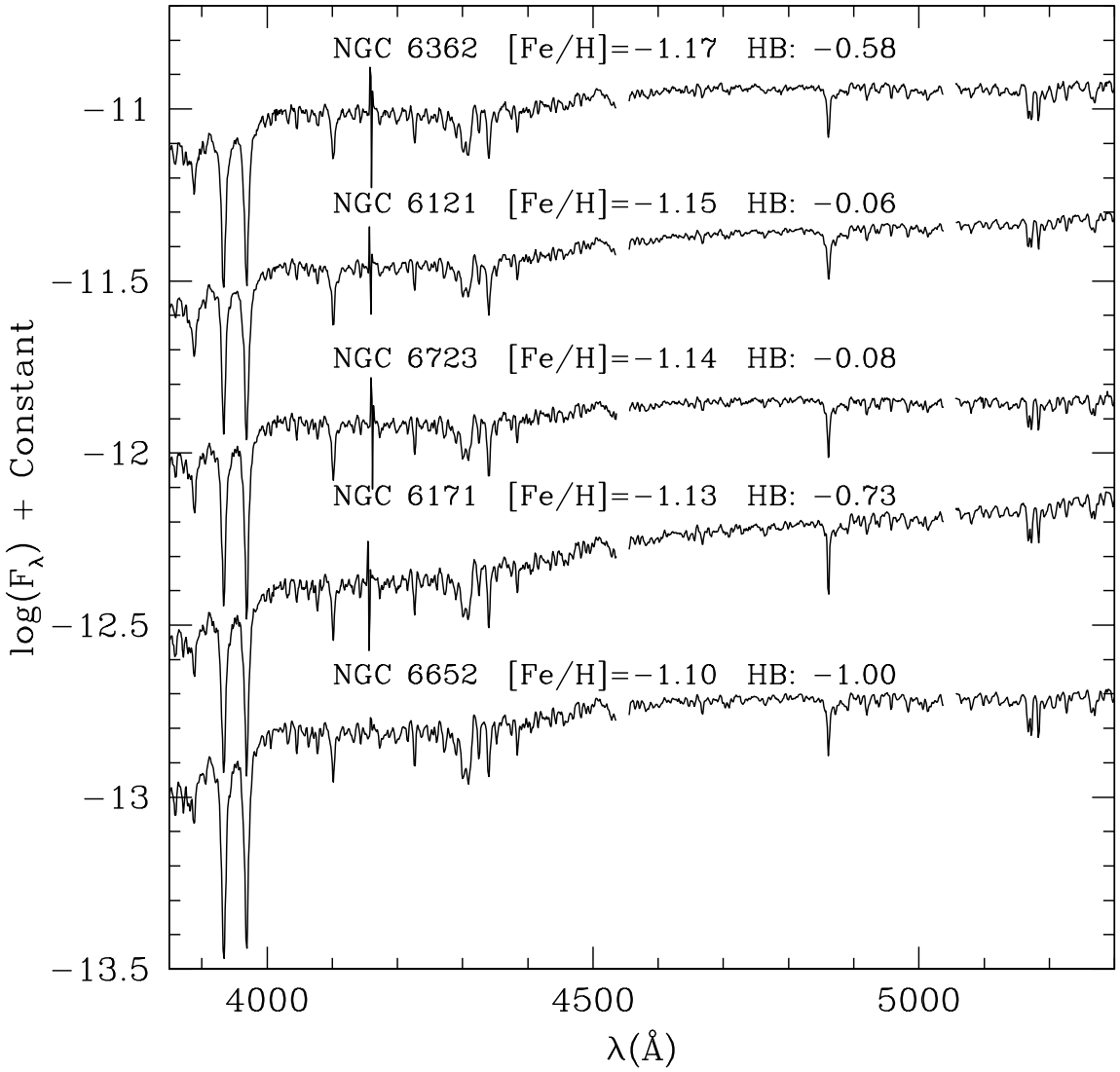
NGC 6362 [Fe/H]=−1.17 HB: −0.58
NGC 6121 [Fe/H]=−1.15 HB: −0.06
NGC 6723 [Fe/H]=−1.14 HB: −0.08
NGC 6171 [Fe/H]=−1.13 HB: −0.73
NGC 6652 [Fe/H]=−1.10 HB: −1.00
−11
−11.5
−12
−12.5
−13
−13.5
4000
4500
5000
λ(Å)
log(F_λ) + Constant

Fig. 2.— e. Cont.

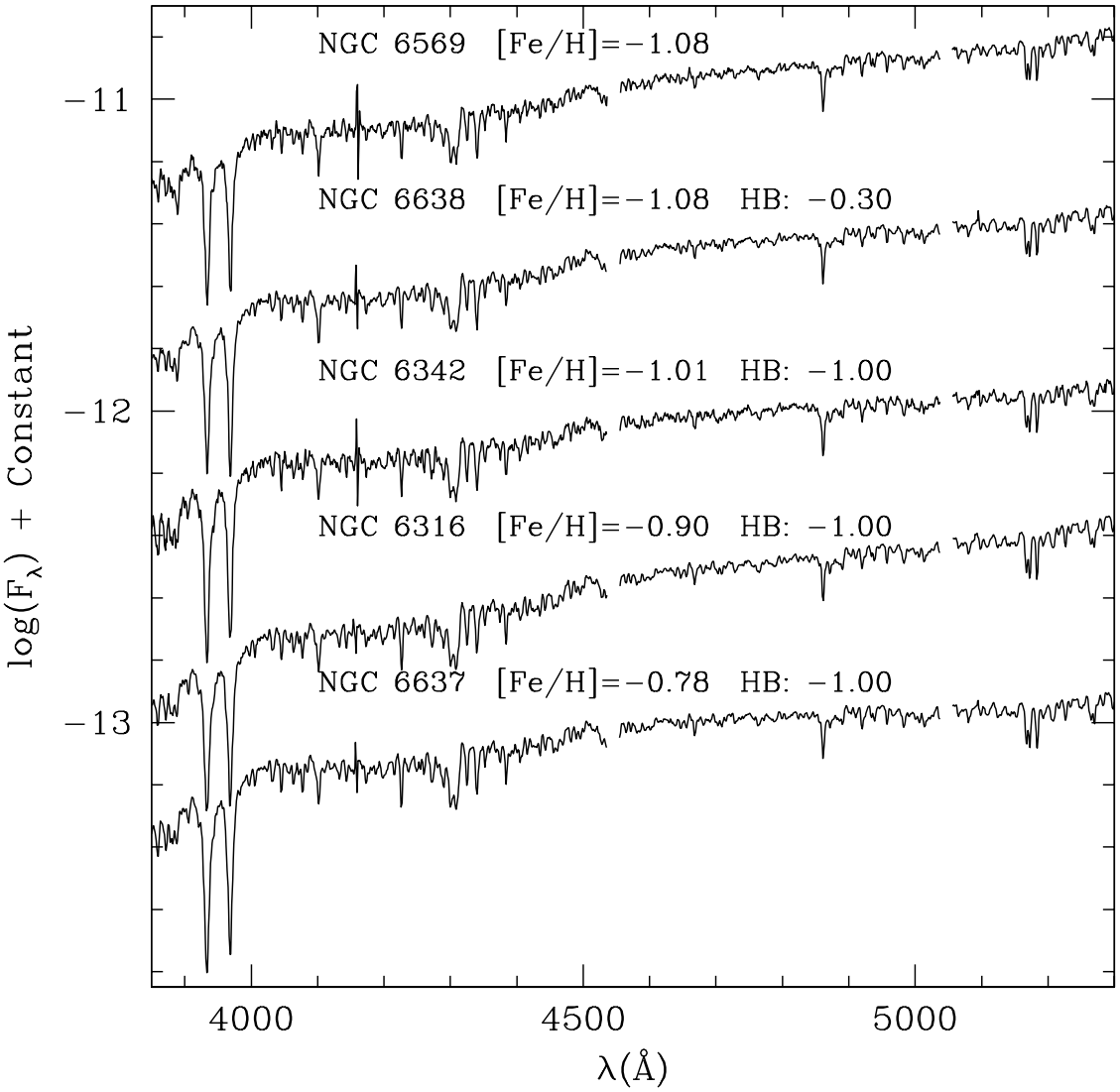
NGC 6569 [Fe/H]=−1.08
NGC 6638 [Fe/H]=−1.08 HB: −0.30
NGC 6342 [Fe/H]=−1.01 HB: −1.00
NGC 6316 [Fe/H]=−0.90 HB: −1.00
NGC 6637 [Fe/H]=−0.78 HB: −1.00
−11
−12
−13
log(F_λ) + Constant
4000
4500
5000
λ(Å)

Fig. 2.— f. Cont.

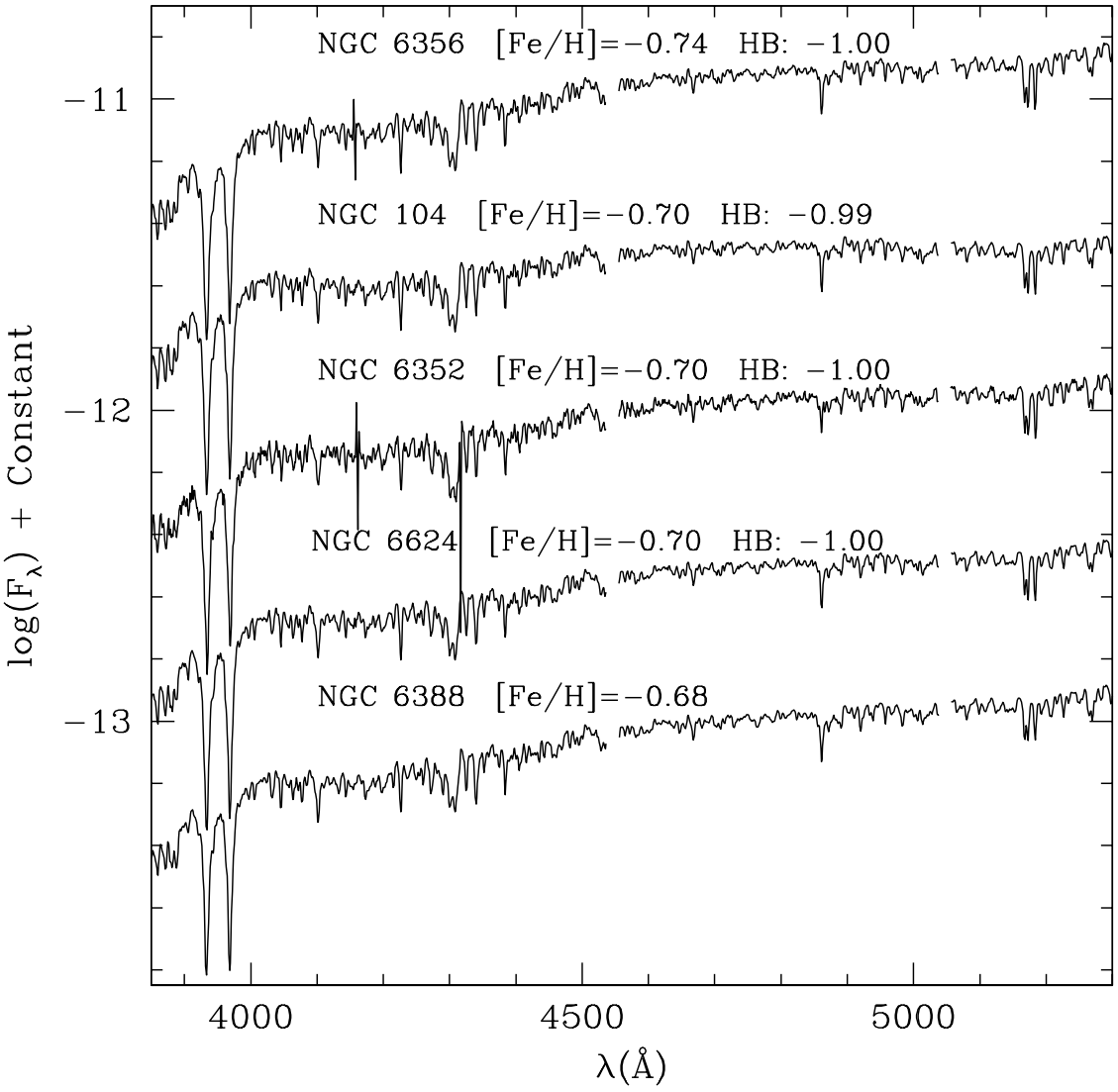
NGC 6356 [Fe/H]=−0.74 HB: −1.00
NGC 104 [Fe/H]=−0.70 HB: −0.99
NGC 6352 [Fe/H]=−0.70 HB: −1.00
NGC 6624 [Fe/H]=−0.70 HB: −1.00
NGC 6388 [Fe/H]=−0.68
−11
−12
−13
log(F_λ) + Constant
4000
4500
5000
λ(Å)

Fig. 2.— g. Cont.

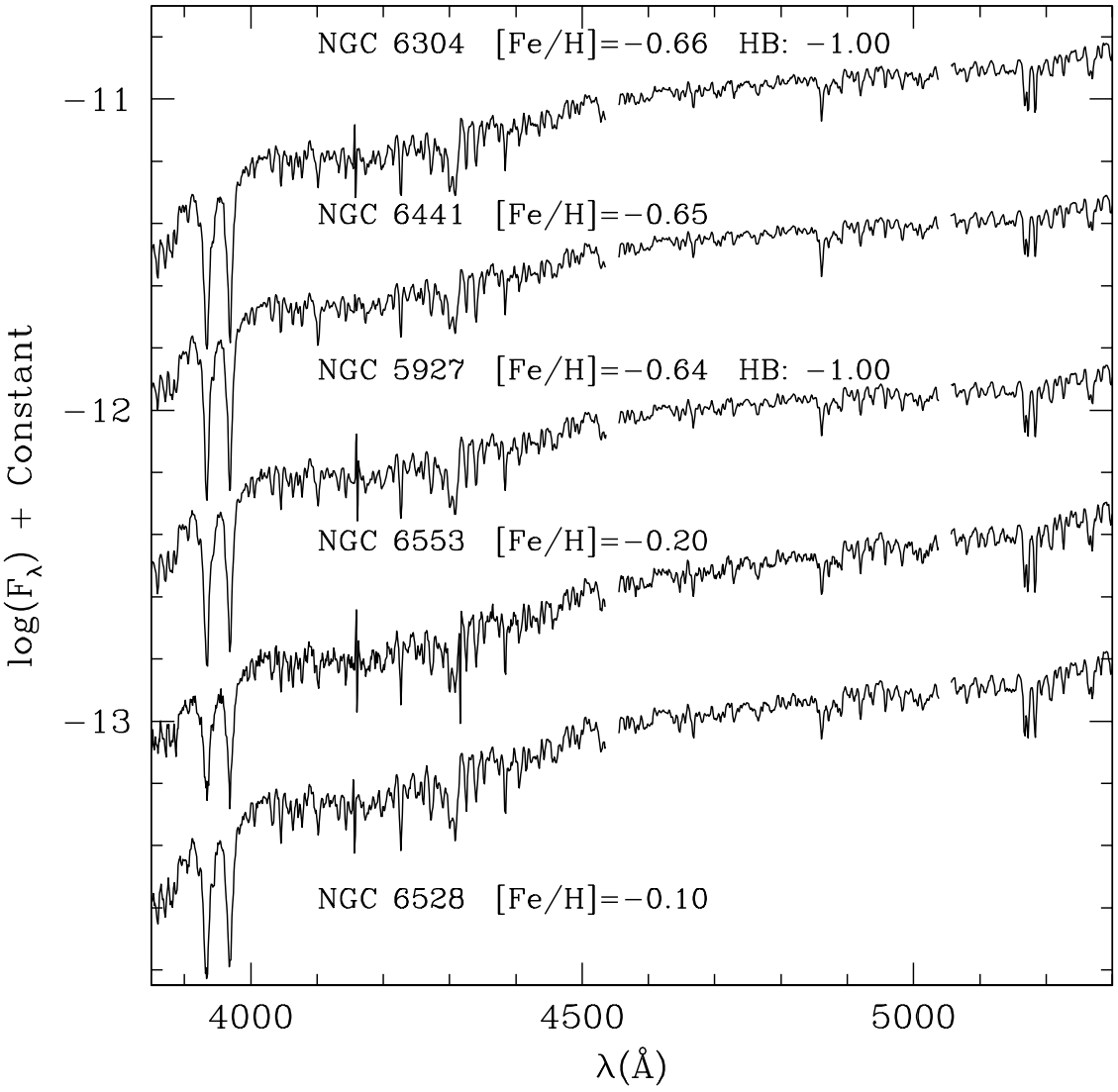
NGC 6304 [Fe/H]=−0.66 HB: −1.00
NGC 6441 [Fe/H]=−0.65
NGC 5927 [Fe/H]=−0.64 HB: −1.00
NGC 6553 [Fe/H]=−0.20
NGC 6528 [Fe/H]=−0.10
−11
−12
−13
log(F_λ) + Constant
4000
4500
5000
λ(Å)

Fig. 2.— h. Cont.

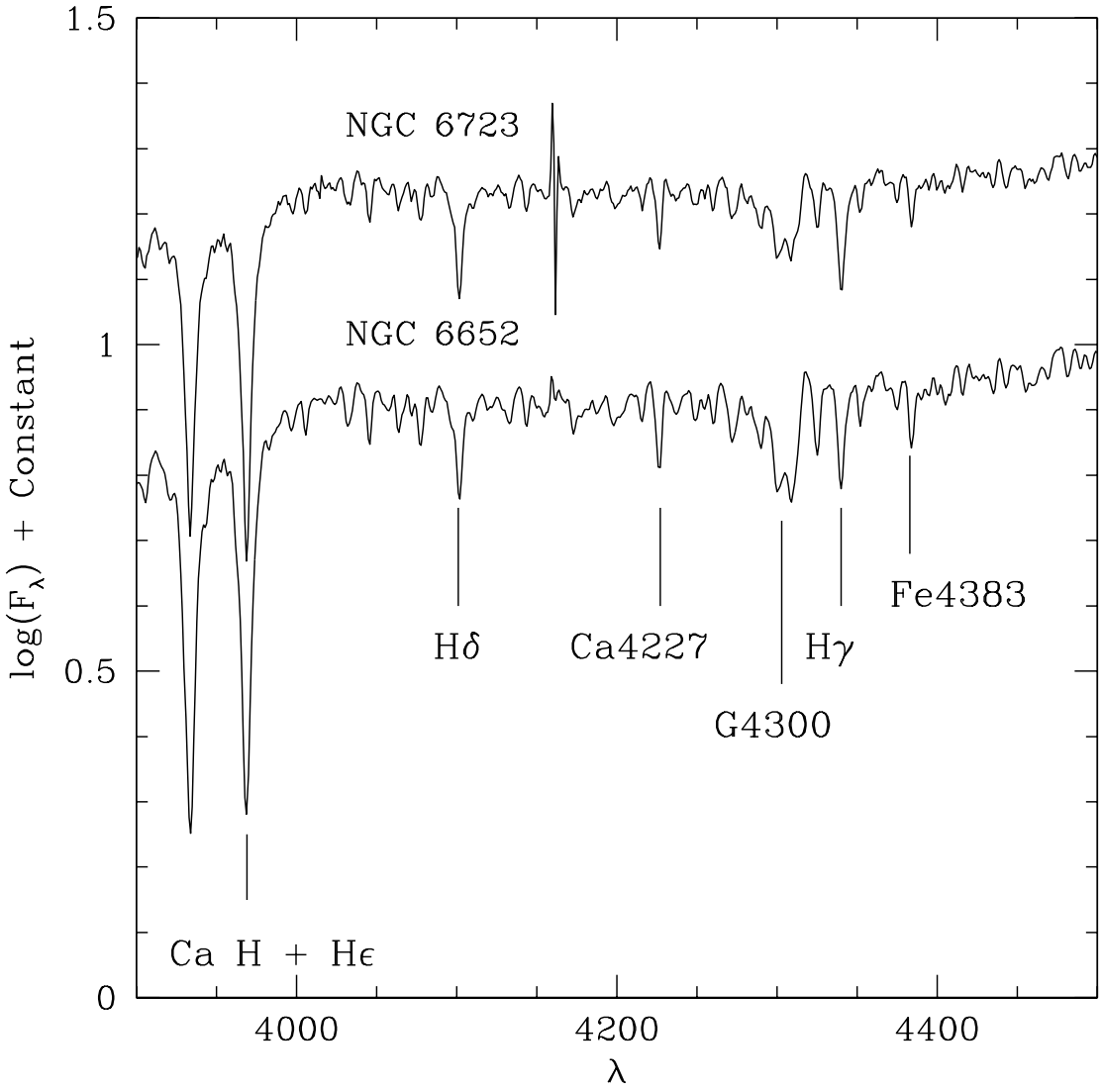

Fig. 3.— Comparison of the integrated spectra of two moderately metal-poor clusters ([Fe/H]∼–1.1) and widely different horizontal-branch morphologies. NGC 6652 has a strictly red horizontal branch, whereas NGC 6723 has a sizeable population of blue HB stars. As a result, Balmer lines are stronger and metal lines are weaker in the spectrum of the latter.

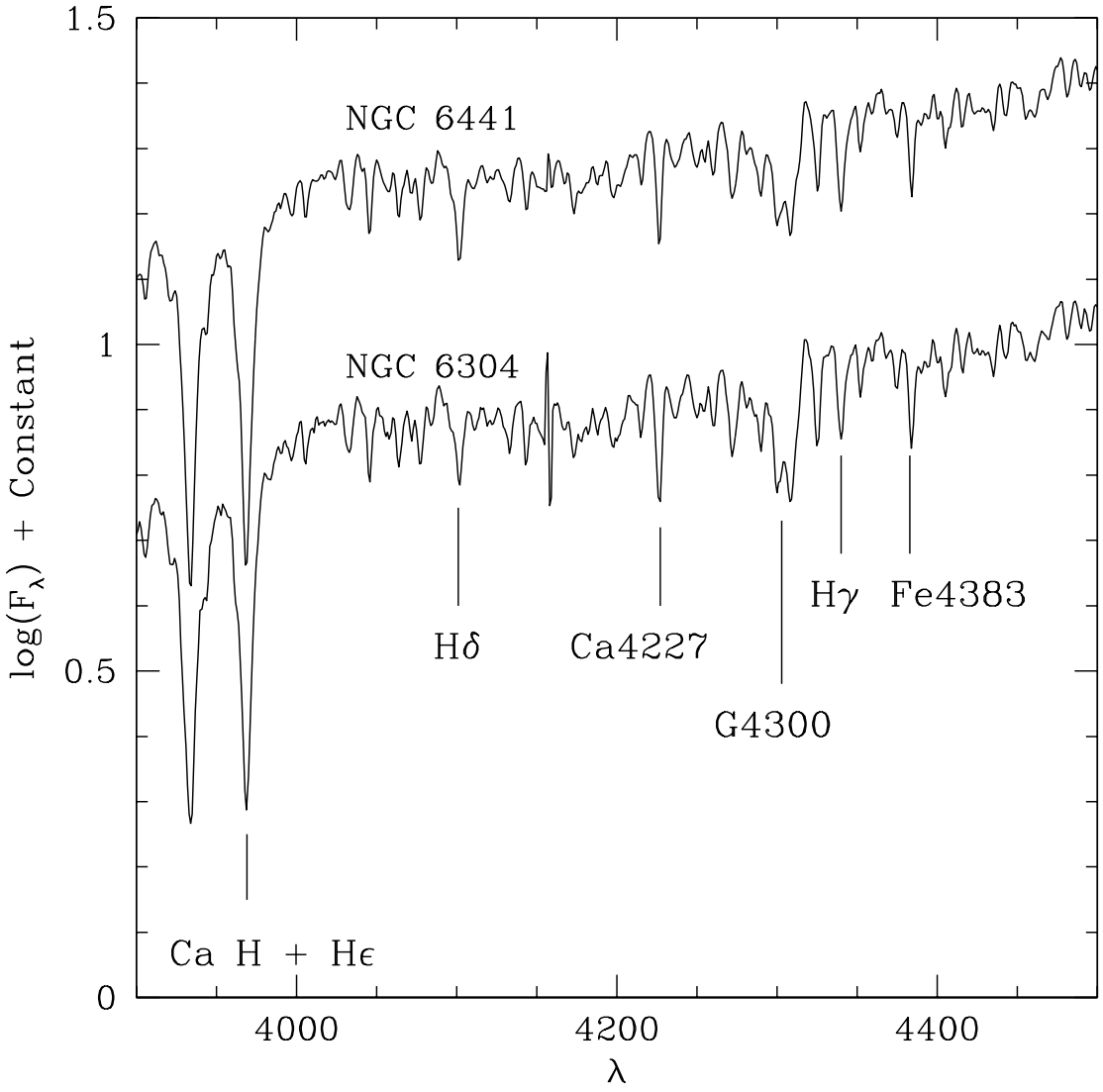

Fig. 4.— Same as Figure 3, now for two metal-rich clusters. While NGC 6304 has a stubby red horizontal branch, that of NGC 6441 is dominated by red stars, but contains a sizeable blue extension. The effect here is more subtle, in that only the Balmer lines are affected, being stronger in the spectrum of NGC 6441. The metal lines are less affected, probably because the horizontal-branch of NGC 6441 has a very strong red component.

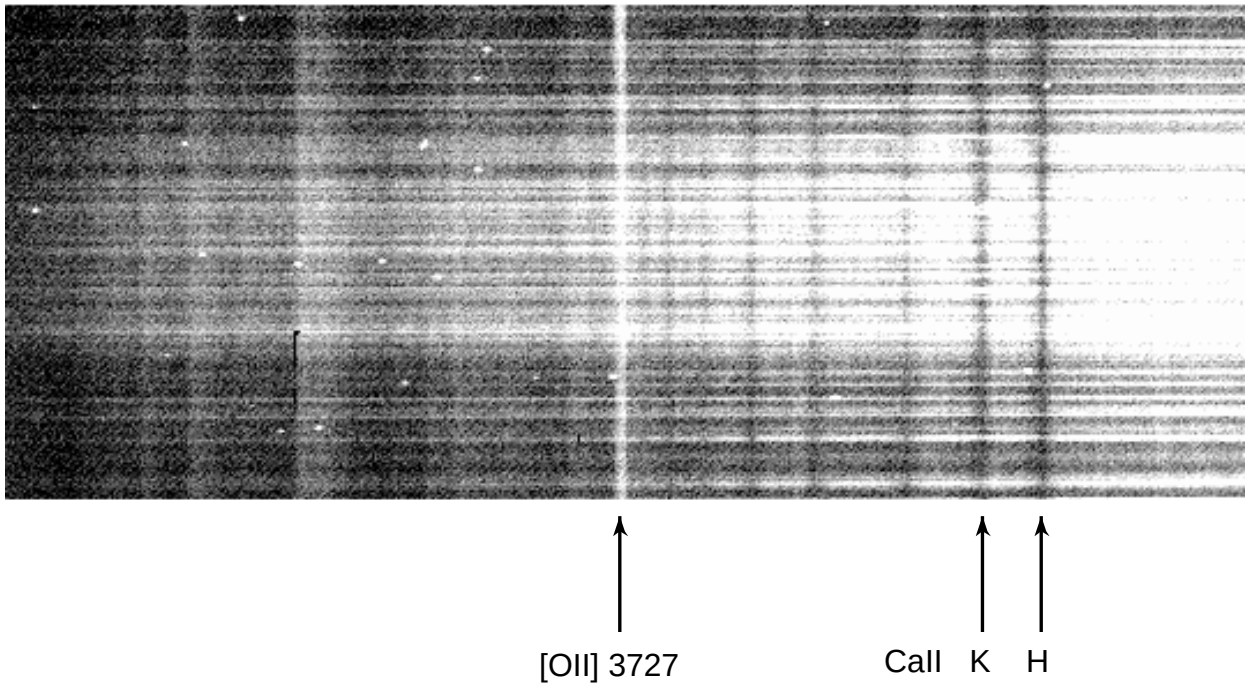

Fig. 5.— Two-dimensional spectrum of NGC 3201. The presence of foreground diffuse emission is indicated by the [O II] 3727 line, suggesting that Balmer lines in the cluster spectrum might be contaminated by diffuse emission. Careful background subtraction needs to be performed in order to correctly remove this contamination.

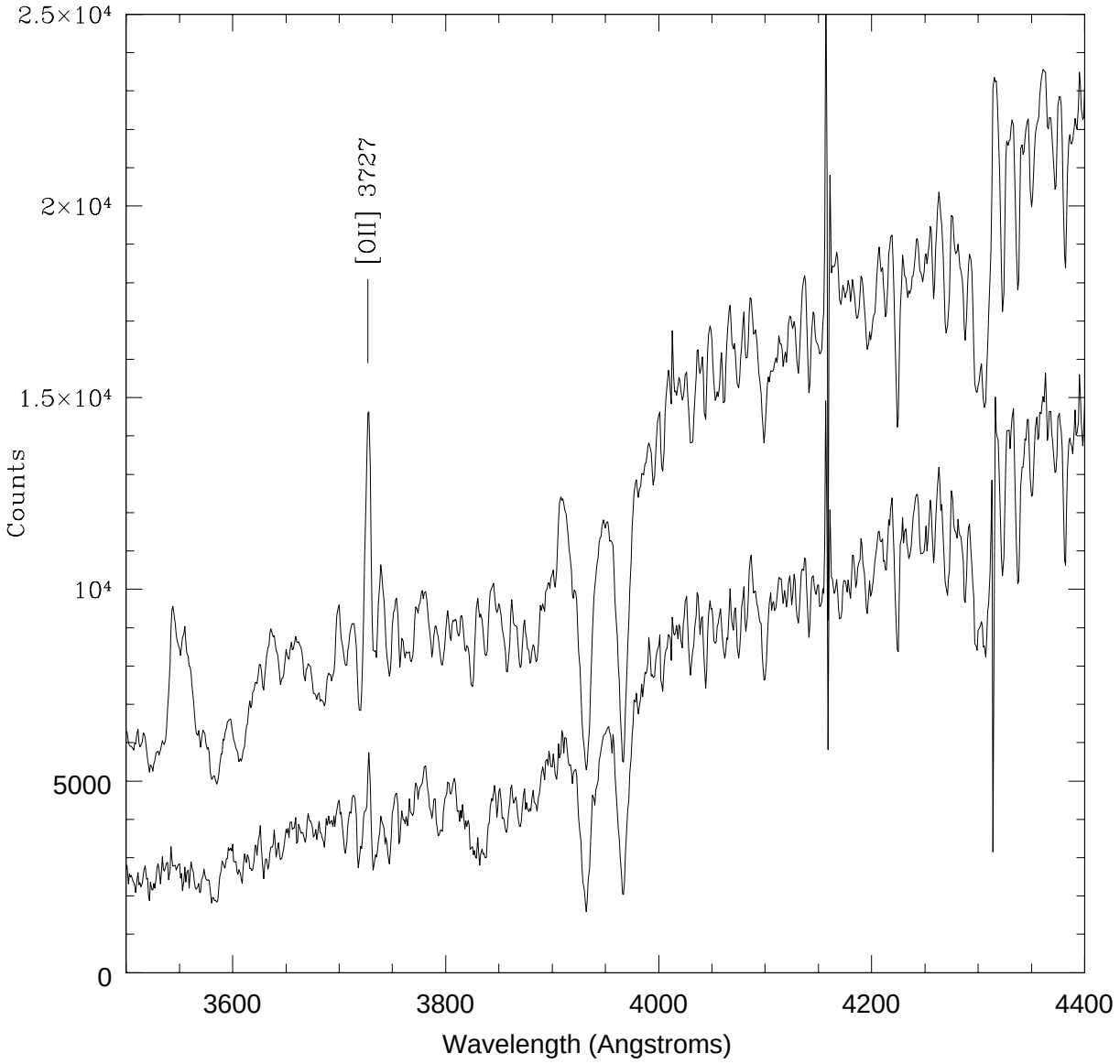

Fig. 6.— Another example of contamination by diffuse foreground emission. Plotted are the spectrum of NGC 6352 before (top) and after background subtraction. Note the very strong [O II] emission line in the top spectrum.

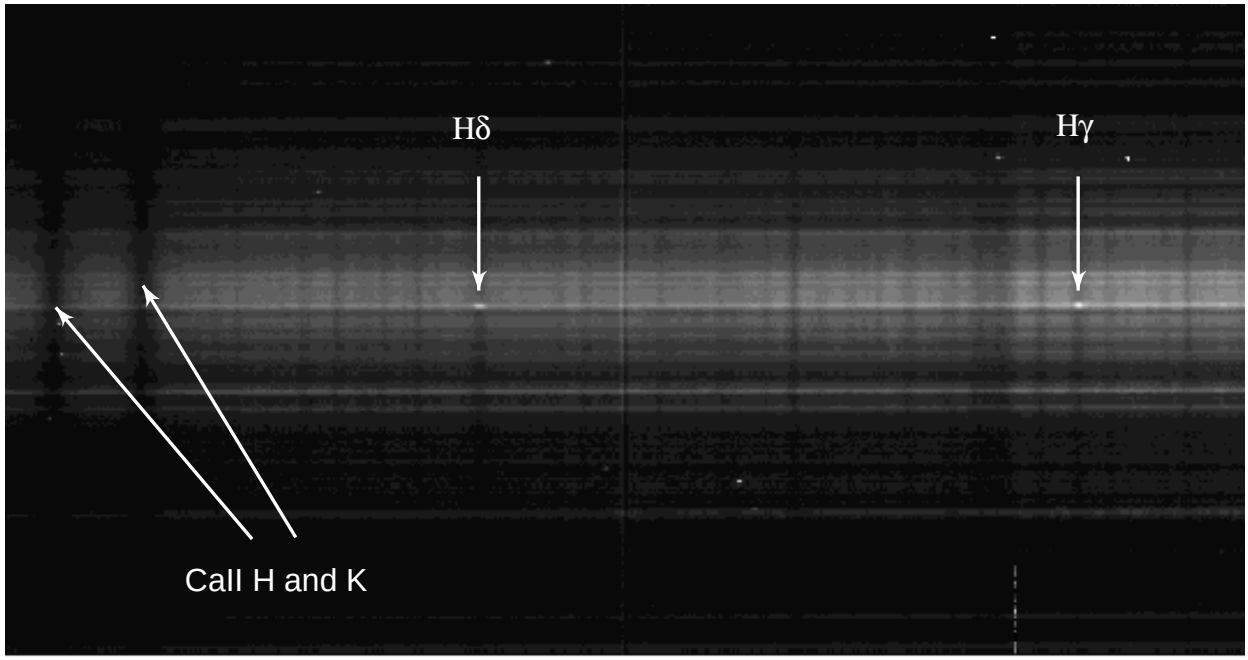

Fig. 7.— Two-dimensional spectrum of NGC 6637. The arrows indicate the presence of emission in both $H\delta$ and $H\gamma$ in a LPV star that was going through an emission-line phase during our observing run.

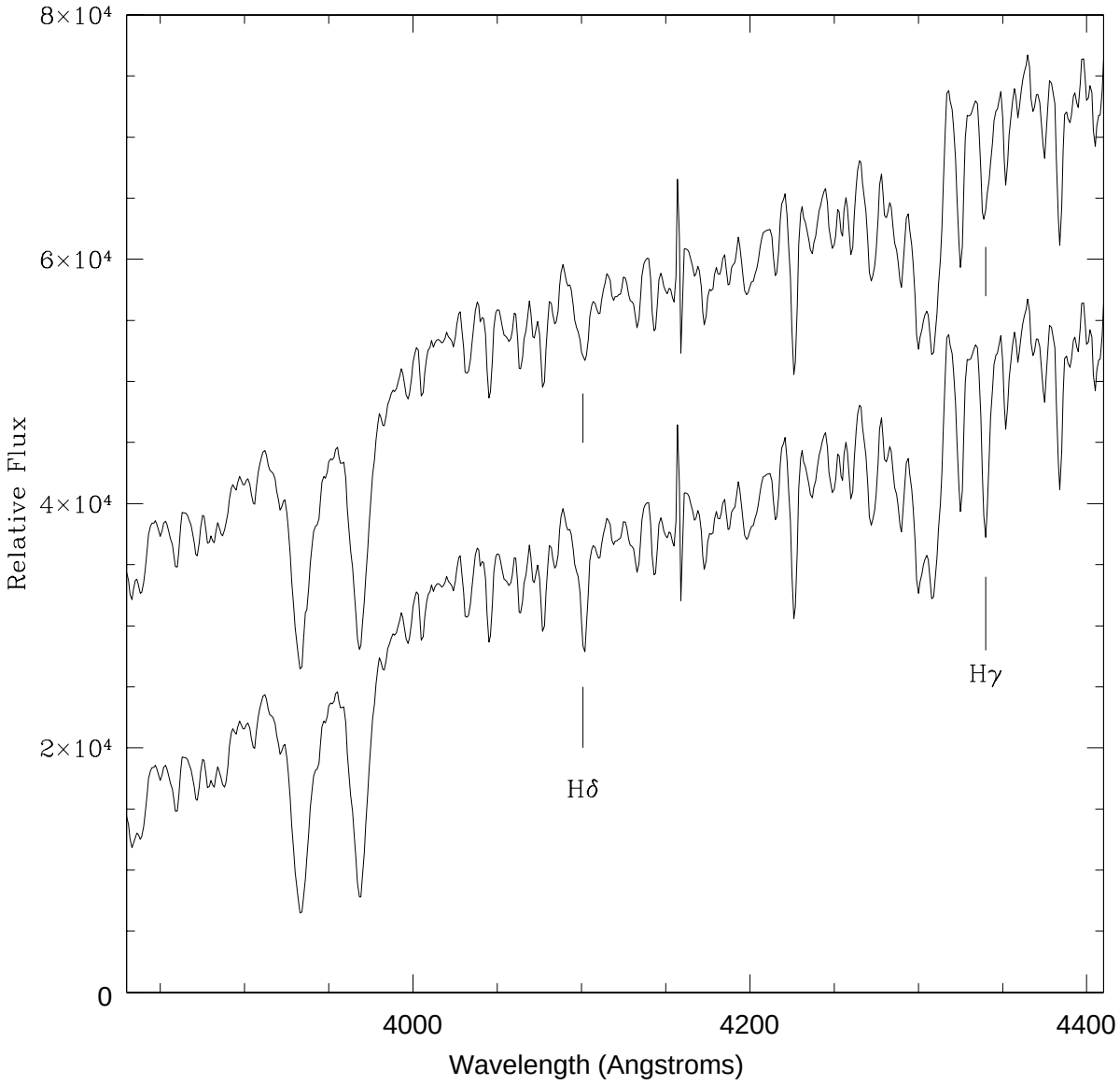

Fig. 8.— One-dimensional spectra of NGC 6637 extracted from the 2-D spectrum shown in Figure 7. In the top spectrum, all the light within the core radius was extracted, and in the bottom spectrum, the LPV star indicated in Figure 7 was excluded from the extraction window. Note the striking difference in Balmer line strengths. Contamination by emission from the LPV makes the Balmer lines much weaker in the top spectrum.